Geoscience Frontiers 6 (2015) 723–740

HOSTED BY

Contents lists available at ScienceDirect

China University of Geosciences (Beijing)

Geoscience Frontiers

journal homepage: www.elsevier.com/locate/gsf

Research paper

Triassic to Cenozoic multi-stage intra-plate deformation focused near the Bogd Fault system, Gobi Altai, Mongolia

Douwe J.J. van Hinsbergen [a,*], Dickson Cunningham [b], Gijsbert B. Straathof [c], Morgan Ganerød [d], Bart W.H. Hendriks [d,e], Arjan H. Dijkstra [f]

[a] Department of Earth Sciences, Utrecht University, Budapestlaan 4, 3584 CD Utrecht, The Netherlands
[b] Department of Environmental Earth Science, Eastern Connecticut State University, Willimantic, CT, USA
[c] SGS Horizon B.V., Stationsplein 6, 2270 JB Voorburg, The Netherlands
[d] Geological Survey of Norway, Center of Geodynamics, Leiv Eirikssons vei 39, 7491 Trondheim, Norway
[e] Statoil ASA, Rotvoll, Norway
[f] School of Geography, Earth and Environmental Sciences, Plymouth University, Plymouth, UK

ARTICLE INFO

Article history:
Received 24 September 2014
Received in revised form
25 November 2014
Accepted 6 December 2014
Available online 23 December 2014

Keywords:
Ar/Ar geochronology
Intra-plate deformation
U/Pb geochronology
Compression
Extension

ABSTRACT

The Gobi Altai region of southern Mongolia has been in the Eurasian plate interior since the mid-Mesozoic, yet has experienced episodic phases of deformation since that time. In this paper, we document field evidence to characterize and date the intra-plate tectonic history of the Gobi Altai region from the Triassic to the present. To this end, we provide detailed mapping of the structure and stratigraphy of the eastern flanks of Mt. Ih Bogd that contains the widest variety of rock-time units in the area. We carry out geochronological analysis of basaltic lavas and basement granite in the area. We demonstrate that a crystalline basement with a 502 ± 8 Ma granitoid (U/Pb) underwent two phases of basin formation in the Mesozoic, which we date with new $^{40}Ar/^{39}Ar$ lava ages of 218.5 ± 1.5, 123.2 ± 0.7 and 124.8 ± 1.2 Ma, respectively. Both phases are linked to deposition of fluvio-lacustrine sediments and trap-like basaltic volcanics, with cumulative thicknesses of 1000–1500 m. Both basins were likely north-facing half-grabens that developed under ~N–S extension, but were subsequently overthrusted by Paleozoic and older crystalline basement during a less well constrained, but likely mid-Cretaceous phase of N–S shortening and basin inversion. Our results are consistent with recent seismic imaging of rift basins ~100 km to the NE of the study area where a similar history was reconstructed. The multiple phases of intra-plate deformation appear to have parallel structural trends, most likely due to reactivated Paleozoic basement structures created during the original terrane amalgamation of the Central Asian Orogenic Belt continental crust. This strong basement heterogeneity may predispose it to reactivation, and make it sensitive to changes in the overall stress field of the Eurasian plate driven by forces at its margins and base. Detailed study of Mongolia's multi-stage tectonic history may thus provide a key proxy for the long-term dynamics of the Eurasian plate. In addition, the repeated reactivation of the Gobi Altai region during the last 200 My supports the contention that non-cratonized continental interior regions composed of Phanerozoic terrane collages are particularly susceptible to fault reactivation, much more than older cratonized continental crust.

1. Introduction

The theory of plate tectonics subdivides the Earth's lithosphere into rigid plates, that move relative to one another along discrete plate boundaries that localize deformation (McKenzie and Parker, 1967; Cox and Hart, 1986). Although the vast majority of plate motion is accommodated along plate boundaries, modern geodetic data, historical earthquake records and study of the geological record of continents reveal that intra-plate deformation is common. The best examples of contractional intra-plate deformation comprise the shortening and uplift history of Tibet (e.g. Dewey et al., 1988; Yin and Harrison, 2000; Kapp et al., 2005; van

* Corresponding author.
E-mail address: d.j.j.vanhinsbergen@uu.nl (D.J.J. van Hinsbergen).
Peer-review under responsibility of China University of Geosciences (Beijing).

http://dx.doi.org/10.1016/j.gsf.2014.12.002

Hinsbergen et al., 2011), Cenozoic inversion tectonics in Central and Western Europe (e.g. Ziegler et al., 1995), and the Cretaceous to Eocene Laramide intra-plate deformation of North America (e.g., Dickinson and Snyder, 1978; Saleeby, 2003). Extensional intra-plate deformation occurs frequently at retreating plate boundaries, forming back-arc rift basins (Jolivet and Faccenna, 2000; Schellart et al., 2007; Faccenna et al., 2014; van Hinsbergen et al., 2014) and where subduction has ceased and slab windows have opened as in North America's Basin and Range province (Dickinson and Snyder, 1978; Saleeby, 2003; McQuarrie and Wernicke, 2005).

Intra-plate deformation in these cases is normally inferred to result from a stress field related to changes in plate coupling at plate boundaries (Molnar and Lyon-Caen, 1988; Vincent and Allen, 2001; Sokoutis and Willingshofer, 2011). This may result from a reorganization of plate boundaries as a result of continent-continent collision, which likely explains intra-plate shortening and inversion in Western Europe (Ziegler et al., 1995) and the Cenozoic uplift of Tibet (Molnar and Tapponnier, 1975), absolute overriding plate motion towards a subduction zone (Oncken et al., 2006), or subduction rollback (Schellart et al., 2007). Although the total amount of strain accommodated by intra-plate deformation normally accommodates a minor fraction of total relative motion at the plate's boundaries, the timing and style of intra-plate deformation may provide key information on the dynamics at the boundaries of the deforming plate.

Central Asia provides Earth's largest example of ongoing far-field intra-plate deformation resulting from continent-continent collision. Since Miocene time, spectacular topographic edifices of the Tian Shan (Yin et al., 1998; Sobel et al., 2006; Jolivet et al., 2010) and the Gobi and western Altai system of Mongolia (Cunningham, 2005, 2010, 2013; Vassallo et al., 2007b; Fig. 1) formed as a far-field expression of stresses transmitted from the collision between the Indian and Asian continents (Molnar and Tapponnier, 1975; van Hinsbergen et al., 2011). In Mongolia, more than 2000 km north of the suture zone between India and Asia, Cenozoic far-field deformation is expressed as transpressional strike-slip tectonics, uplifting restraining bends and thrust ridges (Cunningham et al., 1997; Cunningham, 1998; Bayasgalan et al., 1999b), whose bounding faults in many cases are seismically active (Baljinnyam et al., 1993; Bayarsayhan et al., 1996; Philip and Ritz, 1999; Vassallo et al., 2005; Rizza et al., 2011).

The Cenozoic uplifted ranges in central Asia are parallel to major basement structures that formed at subduction plate margins by accretion of arcs, continental slivers, and ophiolites in Paleozoic to perhaps early Mesozoic time (Sengör et al., 1993; Badarch et al., 2002; Xiao et al., 2004; Lehmann et al., 2010; Wilhem et al., 2012; Rippington et al., 2013). In addition, the upper Cenozoic ranges are flanked by volcano-sedimentary successions that formed at multiple stages throughout the Mesozoic and early Cenozoic (Traynor and Sladen, 1995; Howard et al., 2003; Jolivet et al., 2007; Lamb et al., 2008; van Hinsbergen et al., 2008; Cunningham et al., 2009; Graham et al., 2012; Johnson and Ritts, 2012). The structural context of these basins remains poorly known, but thermochronologic data and stratigraphic evidence indicate that many of the fault zones in the Central Asian basement underwent multiple stages of reactivation (Allen and Vincent, 1997; Cunningham, 2005; Howard et al., 2006; Webb and Johnson, 2006; Jolivet et al., 2010; Webb et al., 2010; Heumann et al., 2014). Studying the structure, stratigraphy and geochronology of the Mesozoic and Cenozoic rock units in the late Cenozoic basement uplifts and along their margins may thus reveal the style and timing of intra-continental, intra-plate deformation in Central Asia, which may serve as a proxy for and constraint on circum-Asian plate boundary processes.

Deformation within Central Asia can be considered to have occurred in an intra-plate position following the early Triassic, when the terranes of Mongolia and China are generally believed to have been fully amalgamated and contiguous with the Tarim and North China cratons to the south, following the closure of the Solonker suture (Xiao et al., 2010; Li et al., 2014). Since then, the Mongolian terranes together with North China converged with Siberia at the expense of the Mongol-Okhotsk ocean, which according to paleomagnetic evidence terminally closed in latest Jurassic to earliest Cretaceous time (Cogne et al., 2005; Van der Voo et al., 2015). Seismic tomographic and magmatic evidence place both Siberia and the Paleozoic terranes of Mongolia in an overriding plate position relative to the Mongol-Okhotsk subduction zones, and this ocean may have undergone oroclinal closure as a result of opposite rotation of Siberia and Mongolia/China, eventually yielding an ENE–WSW trending suture (Van der Voo et al., 1999, 2014; van der Meer et al., 2010; Donskaya et al., 2013). Following latest Jurassic to earliest Cretaceous Mongol-Okhotsk suturing, the nearest plate boundaries were in the Arctic, along the western Pacific margin, and along the northern Neotethyan margin to the south.

In this paper, we document the structure, stratigraphy and geochronology of a series of Mesozoic and Cenozoic volcano-sedimentary deposits flanking Paleozoic crystalline basement exposed in the upper Cenozoic restraining bends of Ih Bogd and Baga Bogd that formed along the Bogd Fault system in the Gobi Altai, southern Mongolia. We use our results to reconstruct a structural history for the Bogd Fault system in terms of extensional, contractional, and strike-slip/transpressional reactivation of the Paleozoic regional basement 'grain', date these events using $^{40}Ar/^{39}Ar$ and U/Pb geochronology, and discuss the geological history in terms of regional tectonic events and plate dynamics.

2. Geological setting and map units

The study area comprises the Ih Bogd and Baga Bogd restraining bends (Figs. 1 and 2), which expose crystalline basement as well as Mesozoic to Cenozoic sedimentary and volcanic rocks that either unconformably overlie the basement, or are juxtaposed against it along faults. Below, we summarize constraints on the nature and age of the local stratigraphy of the study area. Since radiometric age data from samples in the study area are sparse, we also include regional constraints on the age and nature of sedimentary basins, while remaining aware that sedimentary facies may not be regionally contiguous or synchronous.

We mapped units based on lithological characteristics and cross-cutting relationships. Rather than defining local formation names, we further sub-divide the lithostratigraphy according to published, or newly obtained age information.

2.1. Basement units

Badarch et al. (2002) published a terrane synthesis of Mongolia, and assigned the basement of the Gobi Altai to a forearc or back-arc environment in Cambrian to Permo-Triassic times. Demoux et al. (2009) showed that the crystalline basement of Baga Bogd includes a much older history, and reported U/Pb zircon ages from gneisses with magmatic protoliths as old as 1700–1500 Ma, a series of granite gneisses with ~980–950 Ma protoliths, and finally dioritic to granitic gneisses of 502–498 Ma. The Cambrian intrusions are interpreted be related to a volcanic arc.

2.2. Triassic–Jurassic

The geological map of Zabotkin (1988) indicates that the lavas and interbedded terrestrial sediments exposed in the Dulaan Bogd Pass area (Figs. 1 and 2), and extending westwards along the northern flank of Ih Bogd, are Jurassic in age. Jolivet et al. (2007)

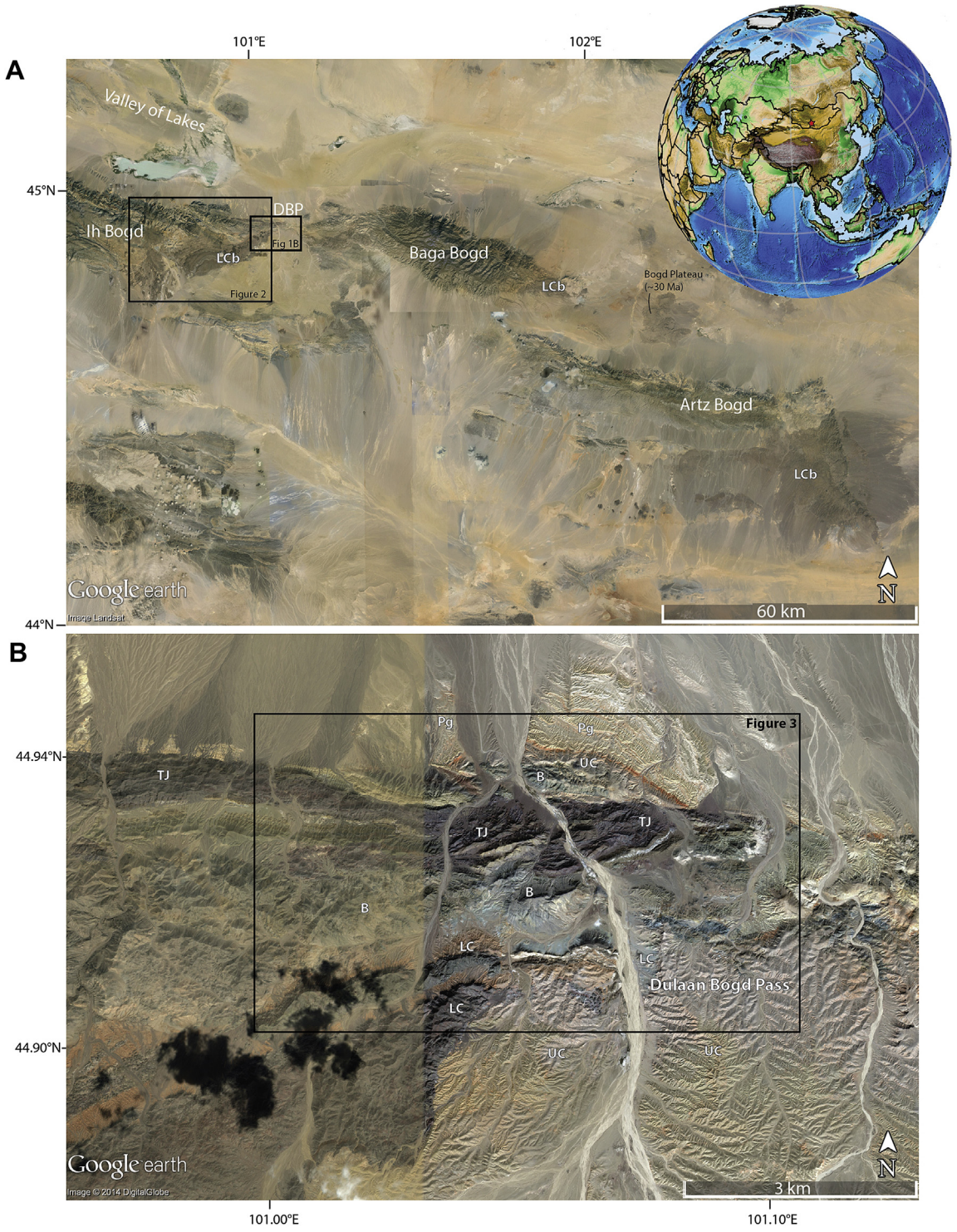

Figure 1. Google Earth images of the study area. (A) Locations of the three main Cenozoic basement-cored uplifts of Mts Ih Bogd, Baga Bogd and Artz Bogd. LCb = Lower Cretaceous basalts. Red star in inset indicates study area. (B) Google Earth image of the Dulaan Bogd Pass area between Ih Bogd and Baga Bogd, highlighting the area that was mapped in detail and shown in Fig. 3. Pg = Paleogene, UC = Upper Cretaceous, LC = Lower Cretaceous, TJ = Triassic–Jurassic; B = Crystalline Basement.

dated mafic lavas from the summit of Ih Bogd to the west, with $^{40}Ar/^{39}Ar$ ages yielding 198 ± 8 Ma and 193 ± 7 Ma (2σ), i.e. earliest Jurassic. Mafic lavas were recently reported from a drill core in the Tugrug basin to the northeast of our study area, which yielded an $^{40}Ar/^{39}Ar$ age of 218.7 ± 0.7 Ma (Johnson et al., 2014). We display this unit on our map as Triassic–Jurassic (TJ), this age designation is also supported by a new, late Triassic $^{40}Ar/^{39}Ar$ lava age that we report in this paper. Jolivet et al. (2007) further showed that apatite fission track ages of rocks from the summit of Ih Bogd are Jurassic ~150 Ma or older. This indicates that the amount of erosion of the summit area has been minimal since the Jurassic, within 1–3 km. Only at the base of Ih Bogd, fission track ages were reset, as a result of late Cenozoic transpression, with an age of 5 ± 3 Ma (Jolivet et al., 2007; Vassallo et al., 2007a).

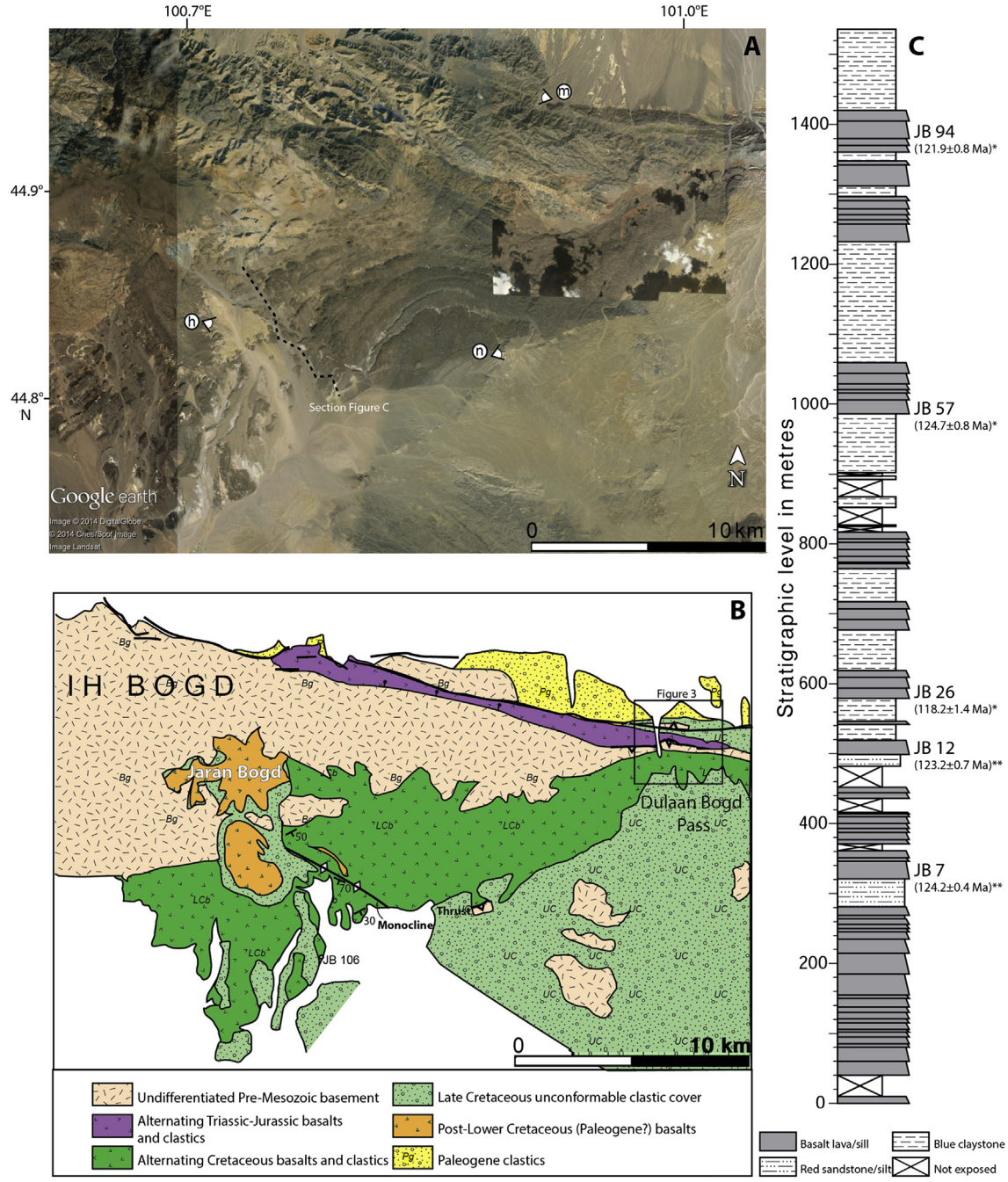

Figure 2. (A) Google Earth image of the eastern part of Ih Bogd showing the succession of dark lava flows and intercalated siliciclastic sediments dipping southeastwards off of the uplifted massif; (B) Geological map of the eastern part of Ih Bogd, modified from Zabotkin (1988); (C) Log of the Jaran Bogd section, with stratigraphic position of $^{40}Ar/^{39}Ar$ basalt ages. Ages indicated with * are taken from van Hinsbergen et al. (2008), ages indicated with ** are newly reported in this paper (see section 4.2). Points j and n refer to view points from which photographs of Fig. 5j and n were taken.

The Triassic to early Jurassic has been considered to be dominated by crustal contraction in the Gobi Altai region (Traynor and Sladen, 1995). However, Meng et al. (2014) demonstrated that the northern margin of the North China craton was under extension throughout late Triassic to early Jurassic time – until (~170 Ma). To the south of the study area, Hendrix et al. (1996), Zheng et al. (1996), Lamb et al. (2008) and Rippington et al. (2013) documented evidence for late Triassic to early Jurassic, ~180 Ma (Guy et al., 2014) contraction in areas ~100–140 km to the south of the study area, and suggested that these stages may form the end of the subduction-accretion history that formed the central Asian crust.

Southeast of the study area, the NE–SW striking, left-lateral East-Gobi fault zone, which yielded $^{40}Ar/^{39}Ar$ cooling ages of ~225–210 Ma (Webb et al., 2010) accommodated as much as 200 km late Triassic slip, followed by another ~100 km in the Oligocene to Miocene (Heumann et al., 2014). The kinematic linkages of this major fault zone to the Triassic closure of the Solonker suture, or Mongol-Okhotsk paleo-plate boundary remain uncertain.

2.3. Lower Cretaceous

Upper Jurassic and Cretaceous terrestrial sediments and mafic lavas are regionally extensive and found across most of the Gobi Desert of Mongolia and Inner Mongolia in northern China, where they are associated with regional, very widely distributed NW–SE extensional basins (Traynor and Sladen, 1995; Hendrix et al., 1996; Graham and Hendrix, 2001; Meng, 2003; Meng et al., 2003; Johnson, 2004; Daoudene et al., 2009, 2012; Ritts et al., 2010; Zhou et al., 2012, 2014; Johnson et al., 2014). In the study area, the basement culminations of Ih Bogd, Baga Bogd, and Artz Bogd are all unconformably overlain by up to 1500 m thick series of lower Cretaceous mafic volcanics interbedded with red to yellow fluvial sandstones and blue-grey lacustrine clay deposits (van Hinsbergen et al., 2008). These sections unconformably overlie Paleozoic and older basement. Published $^{40}Ar/^{39}Ar$ ages of basalts from all three mountainous areas range from 125–115 Ma (Barry, 1999; van Hinsbergen et al., 2008). About 100 km to the northeast of the study area, seismic and borehole data showed evidence for late Jurassic to early Cretaceous formation of a rift basin filled with ~1300 m of fluvio-lacustrine sediments of this age (Johnson et al., 2014). Approximately 150 km to the south of the study area, Cunningham et al. (2009) showed that the western portion of the Altan Uul range exposes a low-angle brittle detachment fault. This fault accommodated NW–SE extension and exhumed low-grade metamorphic basement rocks from beneath folded and faulted Cretaceous sediments. Palynological dating of syn-rift sediments showed that this extension occurred ~120–112 Ma (Cunningham et al., 2009).

2.4. Upper Cretaceous

The study area contains red, clast-supported conglomerates and sandstones that cover all previous units, mapped by Zabotkin (1988) as upper Cretaceous, although no age confirmation has been published from our study area. Regionally, the upper Cretaceous unconformably overlies pre-Cenomanian units. In the East Gobi Basin, as well as ~100 km to the northeast of the study area, evidence was presented for a mid-Cretaceous phase of structural inversion of the upper Jurassic–lower Cretaceous extensional sedimentary basins (Johnson, 2004; Johnson et al., 2014). In the Gobi Altai, the causes of the unconformity and the subsequent re-initiation of sedimentation remain poorly resolved. Farther south, upper Cretaceous strata are well studied because they host world-class dinosaur faunas (e.g., Jerzykiewicz and Russell, 1991; Loope et al., 1998; Van Itterbeeck et al., 2005; Fanti et al., 2012). South of our study area, the upper Cretaceous consists of 500–800 m of fluvial-alluvial conglomerates and sandstones, and aeolian sandstones of Cenomanian to Maastrichtian age (Traynor and Sladen, 1995). We mapped red conglomerates that unconformably cover lower Cretaceous and older units as upper Cretaceous (UC), following Zabotkin (1988).

2.5. Paleogene

The study area contains rocks that were mapped by Zabotkin (1988) as Paleogene. No *in situ* age information is present, but Höck et al. (1999) described Eocene–Oligocene sediments to the north in the Valley of Lakes. These comprise a thin, sequence of clast-supported conglomerates and sandstones interpreted to represent fluvial deposits derived from the Hangay region to the north. In the Valley of Lakes, these fluvial deposits are overlain by brick-red clays and silts with abundant caliche horizons interpreted as aeolian windblown dust deposits (Höck et al., 1999; Vislobokova and Daxner-Höck, 2002; Maridet et al., 2014). $^{40}Ar/^{39}Ar$ ages of basaltic lavas within this unit indicate an early Oligocene deposition (~30 Ma; Höck et al., 1999). To the east of Baga Bogd, a lava plateau of similar age is found (Bogd Plateau; Barry et al., 2003) and an undated lava plateau with similar major element geochemistry and geological characteristics (Dupont-Nivet et al., 2010) unconformably covers tilted lower Cretaceous deposits south of Ih Bogd.

2.6. Bogd Fault

A prominent feature in the study area is the Bogd Fault, along which the Baga Bogd and Ih Bogd restraining bends were uplifted. This fault ruptured in 1957 creating an 8.1 M_W earthquake (Bayarsayhan et al., 1996; Kurushin et al., 1998; Bayasgalan et al., 1999a; Choi et al., 2012). In the Dulaan Bogd pass area, the earthquake ruptured the main E–W trace of the Bogd Fault, and created (or re-activated) ~NNE–SSW trending, WNW-dipping thrust faults known as the Toromhon thrusts (Kurushin et al., 1998; Bayasgalan et al., 1999a).

3. Field results

We mapped the Mesozoic and Cenozoic sedimentary successions that bound the eastern half of the uplifted basement-cored Ih Bogd restraining bend. The map of Fig. 2 is modified from Zabotkin (1988), and shows the regional pattern of major stratigraphic units and structures. In addition we performed detailed mapping of the pass area known as Dulaan Bogd, between the two restraining bends of Ih Bogd and Baga Bogd, where the Bogd Fault system is nearly purely strike-slip (Fig. 3). This area exposes the widest variety of Mesozoic and younger rock units, which are variably deformed. Because no detailed topographic basemap was available, we constructed a map by walking along all contacts between map units and collecting ~900 GPS control points. Below, we describe the lithostratigraphy and structure of the Dulaan Bogd pass area, as well as from the wider volcano-sedimentary stratigraphic successions that flank the eastern margin of the Ih Bogd range.

3.1. Stratigraphy

The Dulaan Bogd Pass exposes crystalline basement covered by and juxtaposed against volcano-sedimentary successions. The crystalline basement comprises greenschists, marbles, and granitoids, and is covered by a sedimentary succession, subdivided into four unconformity bounded units of Triassic–Jurassic, early Cretaceous, late Cretaceous and Paleogene age (Fig. 3). The pass region is subdivided into a central, E–W running basement ridge, separating steeply inclined Triassic–Jurassic strata in the north from shallowly inclined lower Cretaceous strata in the south. Both units are unconformably covered by upper Cretaceous sediments, which are unconformably overlain by Paleogene sediments in the north (Fig. 3).

3.1.1. (Pre-)Cambrian basement

The crystalline basement consists of blue-grey, fine to coarse-grained marbles with white calcite veins (Bc), granite with mafic dikes (Bg) and greenschist facies meta-sediments and meta-volcanics (Bs). The contact between the carbonate and granite units is generally intrusive and a 10 m thick dike of the granite was found intruding the meta-carbonates. The granite is composed of quartz, plagioclase, muscovite, biotite and hornblende, with large (≤10 cm) phenocrysts of K-feldspar (Fig. 4a). The granite is intruded by 50–200 cm wide, abundant blue-grey mafic dikes, sometimes including centimeter scale plagioclase phenocrysts (Fig. 4). These dikes were not observed in the other basement units. The third basement unit (Bs) consists of greenschist facies metasediments

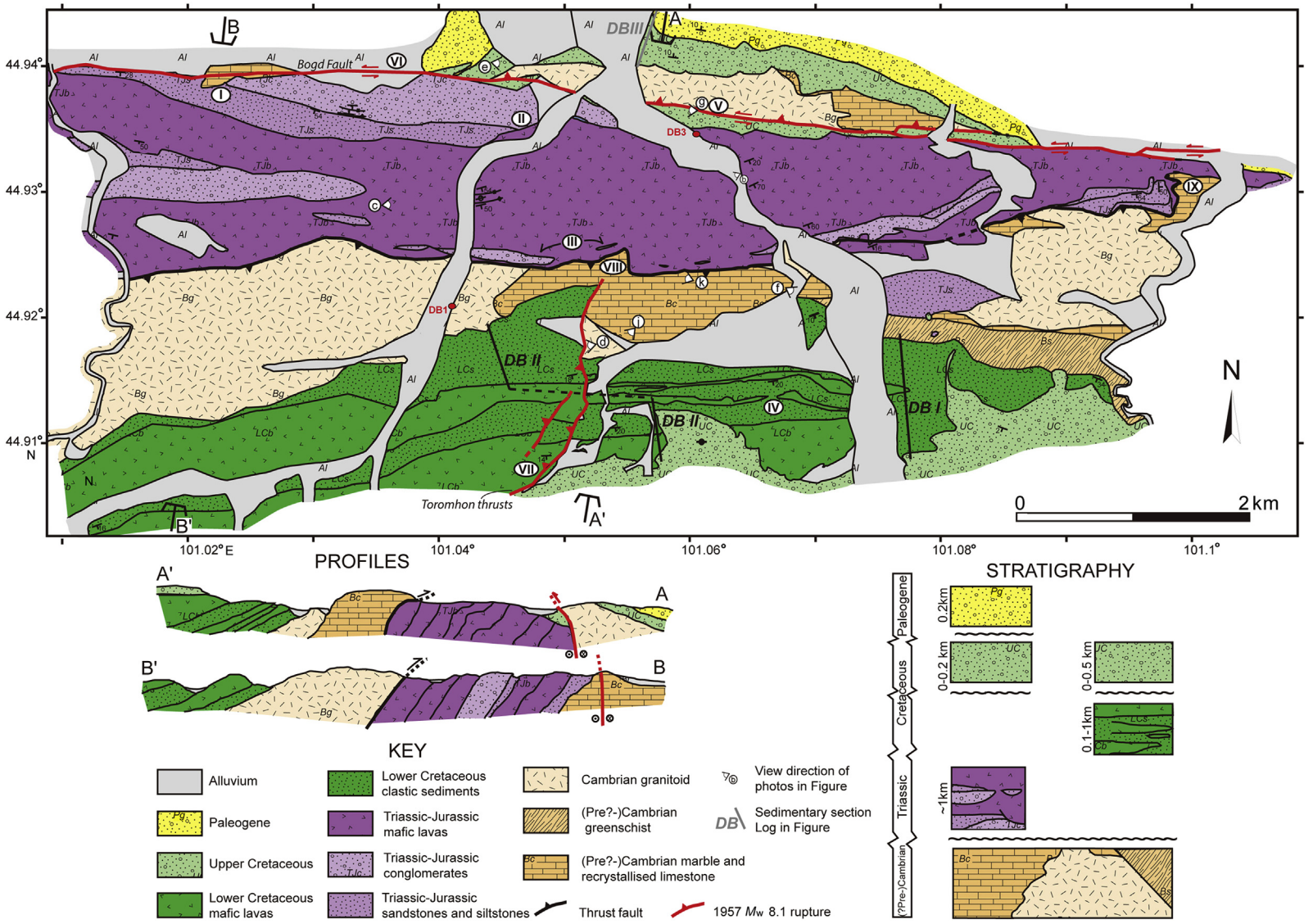

Figure 3. Geological map, cross-sections, and stratigraphy of the Dulaan Bogd Pass area. See Fig. 1 for location. Granite sample from location DB1 and lava sample from DB3 are age dated.

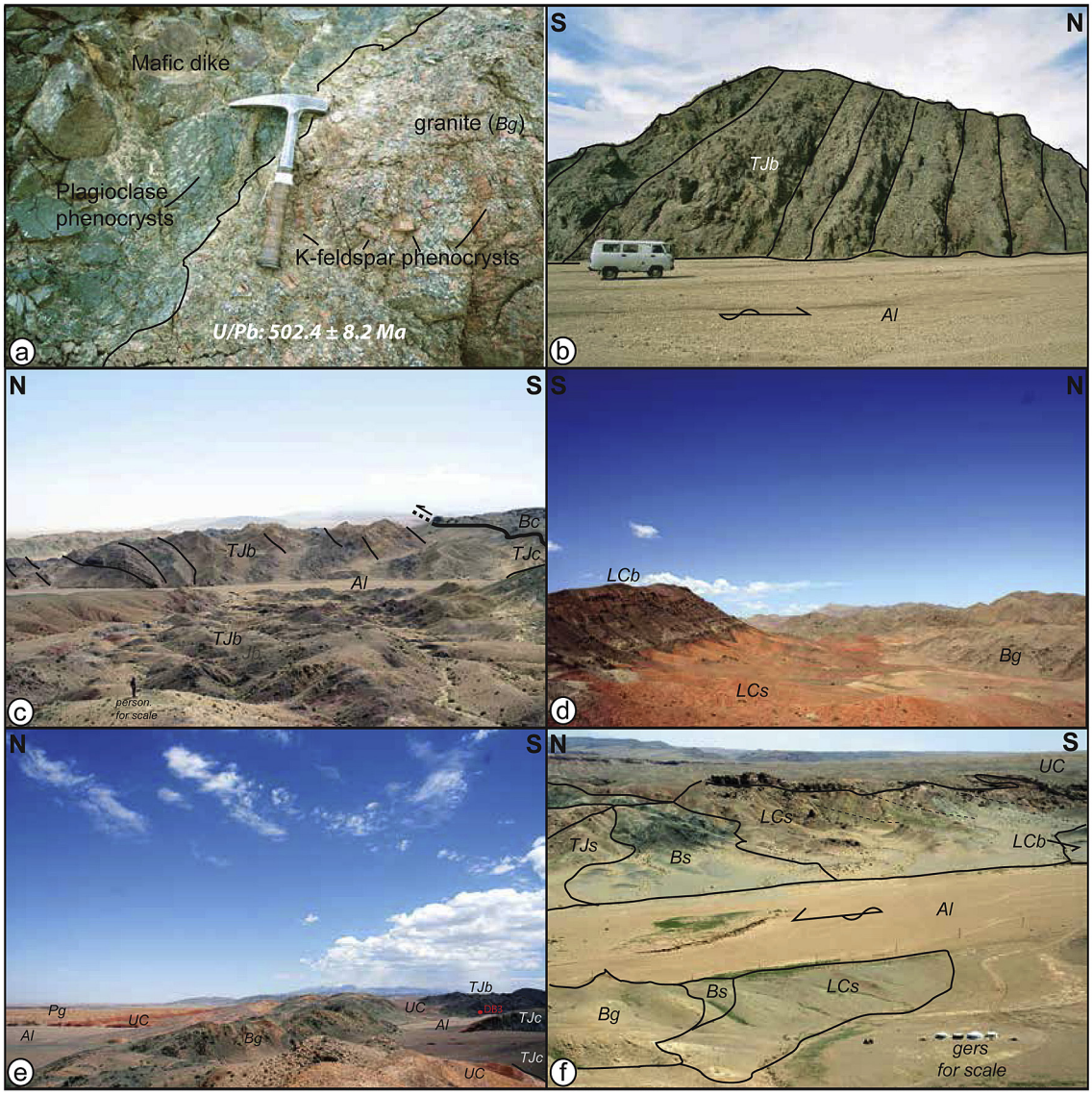

Figure 4. Photographs of key geological features in the study area. For lithological codes, see Fig. 3. Locations of the photographs are indicated in Figs. 3 and 4. (a) Intrusive relationship of mafic dykes into granitoids in the crystalline basement of the Dulaan Bogd Pass area. The granitoid in the photography is dated in this paper at 502 ± 8 Ma (U/Pb); (b) Steeply dipping Triassic–Jurassic basalt lavas. Arrow in river bed indicates flow direction; (c) Eastward view on the Triassic–Jurassic basin in the northern half of the Dulaan Bogd Pass; (d) Base of the Cretaceous sequence in the south of the study area; redbeds and intercalating mafic lavas unconformably overlie crystalline basement rocks; (e) Upper Cretaceous and Paleogene rocks unconformably overlying crystalline basement rocks in the north of the study area; Sample location of DB3 for $^{40}Ar/^{39}Ar$ dating indicated in the Triassic–Jurassic lavas; (f) Upper Cretaceous clastic sediments unconformably overlying crystalline basement rocks as well as lower Cretaceous lavas and redbeds. Arrow in river bed shows flow direction; (g) Upper Cretaceous red beds unconformably overlying Triassic–Jurassic rocks, overthrusted by basement rocks along the 1957 Bogd Fault rupture. Arrow in river bed shows flow direction; (h) View on the monocline deforming the lower Cretaceous lava sequence in the Jaran Bogd area; (j) Basal lower Cretaceous sequence with redbeds and mafic lavas in the Dulaan Bogd area, cut by the 1957 ruptured Toromhon thrust; (k) Crystalline basement overthrusting Triassic–Jurassic sediments and lavas; note that the thrust cuts down-section, suggesting that southward bedding tilt must have been established prior to thrusting; (m) Eastward view on the Triassic–Jurassic basin in between two basement ridges in the northwest of the study area. The geomorphology suggests the presence of normal faults along the southern margin; (n) Crystalline basement overthrusting the lower Cretaceous lava sequence to the southeast of Jaran Bogd. The lavas in the sequence are dipping southward at a steeper angle than the north-directed thrust, which consequently cuts down-section. This requires a pre-thrusting southward tilt of the lavas. (Continued).

and metabasites, which are locally ductiley sheared in meter-wide shear zones. The contact of this unit with the granite and the metacarbonates is – where observed – pervasively sheared. A detailed analysis of the crystalline basement is beyond the scope of our investigation, but we collected a sample from the granite (DB 1) for U/Pb zircon dating.

3.1.2. Mesozoic–Cenozoic sedimentary cover

3.1.2.1. Triassic–Jurassic units TJb, TJc and TJs. The oldest volcano-sedimentary sequence consists of a series of clastic sedimentary and mafic volcanic rocks with a maximum exposed thickness of approximately 1500 m, 90% of which consists of lavas, covering the central-northern part of the mapped area (Fig. 3). The sequence dips 50–70° S (Fig. 4b). In the northwest of the study area (point I in Fig. 3) a steeply southward tilted unconformable contact between basement marbles and sandstones and conglomerates of this sequence was found. Everywhere else, the contact of the TJ units with basement is faulted. In the south, the TJ units are overthrusted by basement, and to the north it is separated by the Bogd Fault (Fig. 4). Three lithologies are separately mapped: mafic lavas (TJb), conglomerates (TJc) and sandstones-siltstones (TJs). The mafic volcanic series comprises lavas up to 20 m thick.

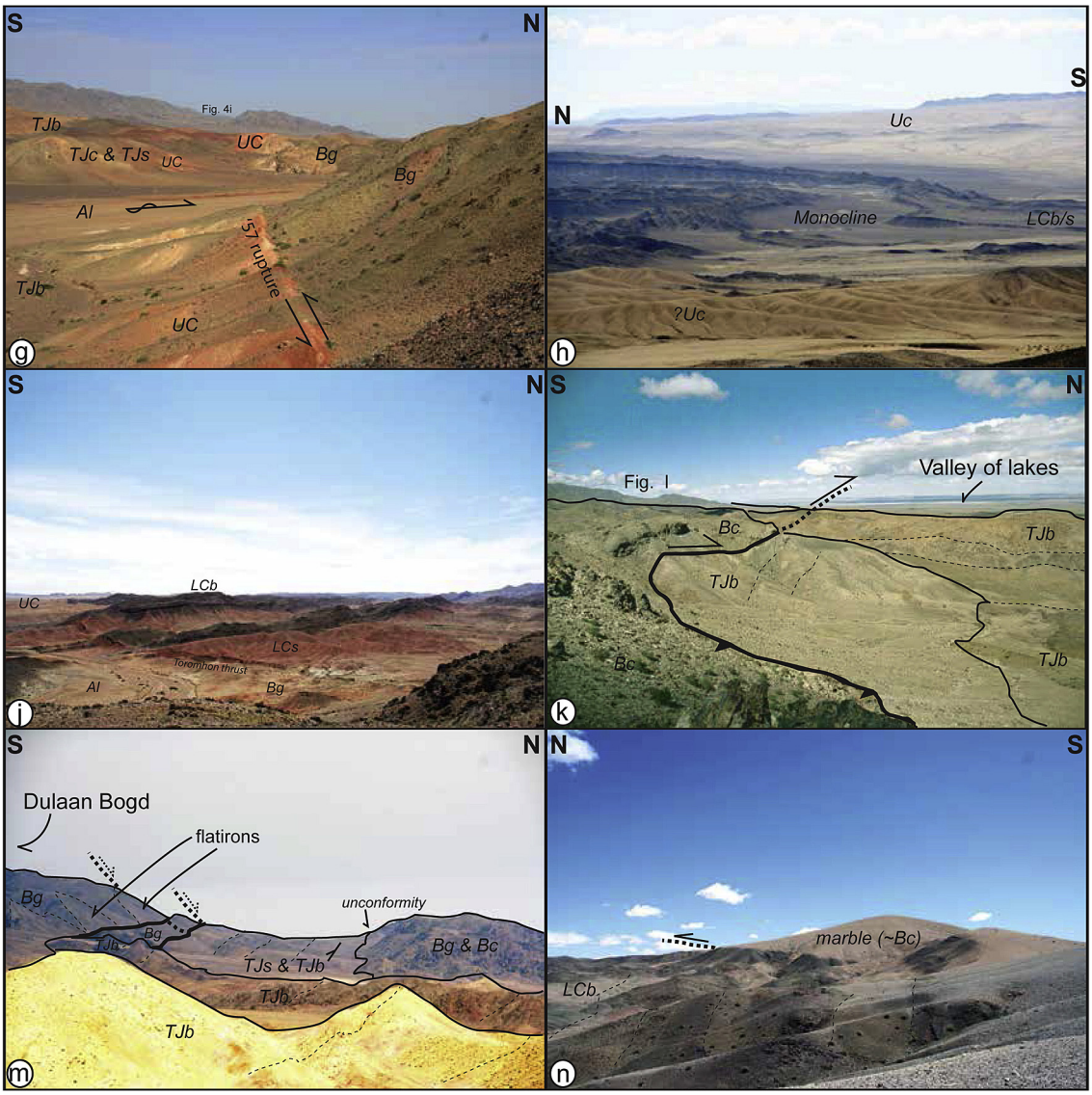

Figure 4. (*continued*).

Individual lavas can be followed laterally over at least hundreds of meters. We collected sample DB3 for $^{40}Ar/^{39}Ar$ dating at the base of the volcanic stratigraphy (Figs. 3 and 4).

Conglomerates and sandstones form lens-shaped bodies embedded in siltstones; the sandstones commonly contain cross-bedding. We interpret these rocks as fluvial deposits. Intercalations of clastic sedimentary rocks within the thick lava succession thicken and increase towards the west. In the center of the mapped area, an intraformational angular unconformity separates lava from underlying conglomerates and sandstones (Point II in Fig. 3) in a paleo-channel.

The southern, stratigraphically highest part of the sequence is characterized by abundant intercalations of lens-shaped conglomerate bodies with a thickness of up to tens of meters and a width of up to ~100 m (Point III in Fig. 3). These conglomerates are clast-supported, and mainly composed of poorly rounded, coarse boulders, cobbles and gravel of up to 50 cm across, consisting of granites with large K-feldspar phenocrysts as well as blue-grey marbles, closely resembling those of the adjacent basement units Bg and Bc. Paleocurrent directions could not be determined from these lenses, but it seems reasonable to interpret the sequence as proximal alluvial fan deposits, with boulders derived from the basement units that are now thrust on top of the Triassic–Jurassic sequence (Fig. 3).

Sparse paleocurrent directions observed while mapping the sandstones are between south and west-directed. This, in combination with the westward increase of (exposed) thickness, and increasingly thick intercalations of clastic sediments suggests a westward and southward increase in accommodation space. The modern southern margin of the Triassic–Jurassic basin was likely also close to the paleomargin, given the proximal fan-deposits are likely derived from the adjacent basement units. Regionally, the Triassic–Jurassic units can be followed ~10 km westwards, where they crop out in a narrow valley between two basement ridges (Fig. 2).

3.1.2.2. Lower Cretaceous units LCb and LCs. In the south of the Dulaan Bogd Pass area, crystalline basement is unconformably overlain by ~20° SSE dipping alternating red clastic sedimentary rocks (LCs) and mafic lavas with abundant, large amygdules (≤20 cm; LCb; Fig. 4d). In the map area of Fig. 3, the exposed thickness of the lower Cretaceous series is only 100–200 m (Fig. 5),

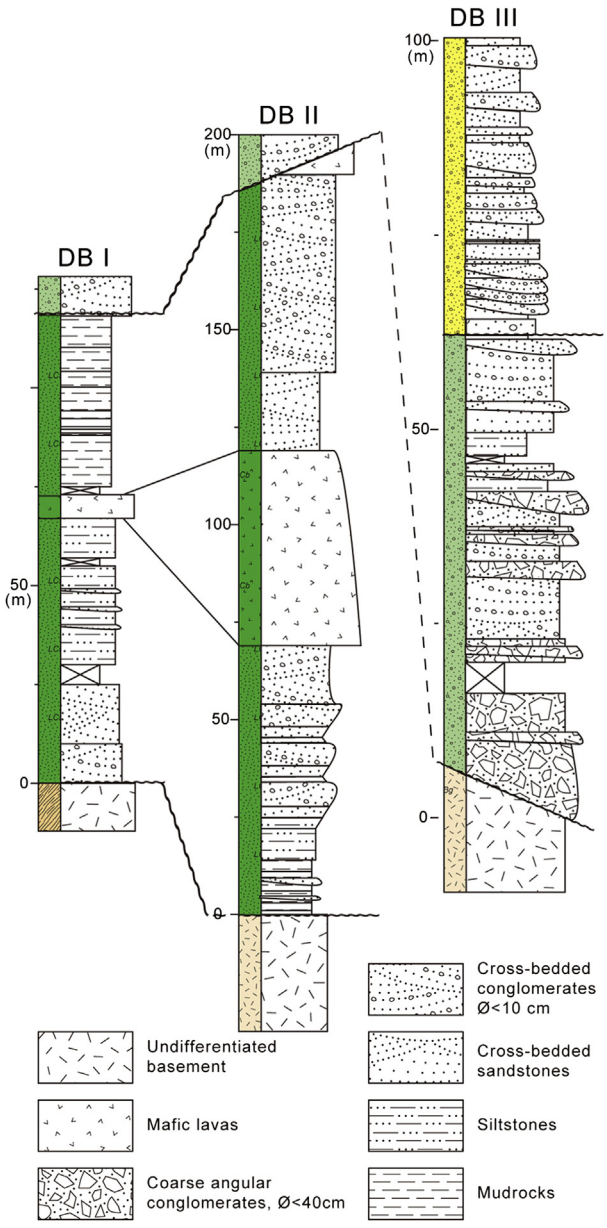

Figure 5. Sedimentary logs of the Cretaceous and Paleogene of the Dulaan Bogd Pass area. No log is presented for the Triassic–Jurassic rocks which comprise a ~1.5 km thick succession consisting of 90% basaltic lava. For locations of the sections, see Fig. 3.

but this thickness increases westward, reaching ~1500 m in the Jaran Bogd area (van Hinsbergen et al., 2008; Fig. 2). This is not only due to the unconformable overlap of the lower Cretaceous sequence by upper Cretaceous sedimentary rocks. In the study area, the lower Cretaceous lavas become thinner and eventually disappear entirely towards the east, both in individual flow unit thickness and in overall stratigraphic thickness (Fig. 3). This suggests larger accommodation space in the west than in the east.

In the mapped area, the basalts are clearly extrusive, as can be shown by baked contacts at the base of the lavas, but not at the top. In the Jaran Bogd section farther to the west, previous $^{40}Ar/^{39}Ar$ ages of 124.7 ± 0.8 Ma and 121.9 ± 0.8 Ma were obtained for basalts that are at stratigraphic levels of ~1000 m and ~1400 m above the crystalline basement, respectively (van Hinsbergen et al., 2008). A younger age of 118.2 ± 1.4 Ma was obtained from a basalt that is stratigraphically ~600 m above basement, which was interpreted as younger sill intruded into the older lava sequence (van Hinsbergen et al., 2008). We explored whether this section would provide an opportunity for calibrating a palynological timescale, for which purpose we dated another two basalts (JB7 and JB12) by the $^{40}Ar/^{39}Ar$ method, at ~350 and ~500 m above basement in the base of the section, respectively. The results of the palynological analyses and time scale calibration are beyond the scope of this paper and are being prepared for publication elsewhere.

The lower Cretaceous sedimentary rocks in the Dulaan Bogd Pass area are restricted to the base of the succession, and unconformably overlie and are derived from the local crystalline basement. The deposits are variable in grain size from conglomerates (grain size ≤ 10 cm) to bright-colored greenish, blue-grey, purple and red mudrocks. Sandstone lenses show southerly paleocurrents, in line with a sediment provenance from the northern basement. No evidence was found for reworking of Triassic–Jurassic or any other lavas in the conglomerates, suggesting that the Triassic–Jurassic succession was not exposed and available for erosion during the early Cretaceous.

3.1.2.3. Upper Cretaceous and Paleogene conglomerates. A formation of red, clast-supported conglomerates and sandstones is found in unconformable contact with all basement units, and the Triassic–Jurassic lavas and sedimentary rocks, as well as the lower Cretaceous units. We have no independent age constraint for these rocks – samples taken for palynology were barren (D. McLean, pers. comm. 2005), but the map of Zabotkin (1988) assigns these rocks to the upper Cretaceous. The formation is certainly not Neogene, as it is unconformably overlain by yellow conglomerates intercalated with brick-red siltstones, which are well-known from the Valley of Lakes area, where they are interbedded with Oligocene lavas (Höck et al., 1999).

Bedding in the upper Cretaceous sedimentary rocks is regionally subhorizontal, and the basal unconformity with the lower Cretaceous lavas and sedimentary rocks can be traced all the way to the Jaran Bogd section (Fig. 2). The maximum exposed thickness of the upper Cretaceous succession in the study area is ~70 m (Fig. 5), but owing to its horizontal orientation and the regional low relief, this must be considered a minimum.

The upper Cretaceous rocks contain clasts derived from all crystalline units, as well as mafic magmatic rocks that resemble the lower Cretaceous and Triassic–Jurassic lavas they unconformably overlie. In the Dulaan Bogd Pass area, such red, poorly sorted, coarse, and angular conglomerates are exposed in the north, unconformably overlying basement and Jurassic lavas (Fig. 4e, g) and in the south, they unconformably overlie the lower Cretaceous sequence (Fig. 4f). Due to the very coarse and proximal nature of these sediments, paleo-flow directions are difficult to obtain, but a few locations of cross-bedded sandstones show flow directions that are north-directed in the north, and south-directed in the south. This suggests that the Dulaan Bogd pass area formed a local high in the late Cretaceous, shedding proximal, angular debris to adjacent lower areas.

Finally, the upper Cretaceous sedimentary rocks are covered by yellow conglomerates with an entirely different facies and composition. These conglomerates were mapped as Paleogene by Zabotkin (1988), are clast-supported, and consist of well-rounded pebbles of mainly white and yellow limestones and sandstones which are not found in any of the underlying units. They have smaller clast sizes than the older surrounding siliciclastic rocks, and their composition and sphericity suggests that they are derived from a much more distal sediment source than the underlying upper Cretaceous rocks. These conglomerates alternate with brick-red siltstones that most likely correlate with similar sedimentary successions from the northern Valley of Lakes that intercalate with

Oligocene lavas (Höck et al., 1999). The sequence exposes well-defined erosional channel fills and are in places intercalated with thin evaporite and sand deposits. Paleocurrent-directions obtained from pebble imbrications and cross-bedded sandstones are invariably south to southeast-directed, indicating that the Dulaan Bogd Pass region did not form a sediment source, nor a topographically elevated area in the Oligocene. The contact between the upper Cretaceous and Paleogene is sharp, subparallel to bedding, and the units never intercalate. The contact between the two units is therefore a disconformity. We only observed these yellow distal conglomerates in the northern part of the Dulaan Bogd Pass area.

3.2. Structure

The present-day structure of the Dulaan Bogd Pass region is mainly characterized by a number of thrusts and transpressional strike-slip faults. In the north, the region exposes the E–W running, left-lateral Bogd strike-slip fault that ruptured during the 1957 earthquake (Baljinnyam et al., 1993; Bayarsayhan et al., 1996; Bayasgalan et al., 1999a). In places, the fault is transpressional and brings crystalline basement southward over Triassic–Jurassic and upper Cretaceous units along steep oblique-reverse faults (Point V in Fig. 3; Fig. 4g). In the uppermost part of the crust, this fault may locally follow the unconformity between the Triassic–Jurassic sedimentary units and the crystalline basement (e.g. around point I in Fig. 3). In other places, no large offset can be seen along the fault, and its expression remains restricted to a small scarp in recent alluvium (e.g., Point VI in Fig. 3). It is difficult to assess the amount of displacement along the fault in the absence of well-defined markers. The Bogd Fault system is ~250 km in length (Florensov and Solonenko, 1963; Bayarsayhan et al., 1996; Cunningham, 2010, 2013) suggesting significant offsets. The comparable lithologies of the basement and upper Cretaceous sediments on either side of the strike-slip fault that ruptured in 1957, however, suggest that this strand has only a minor cumulative offset.

Other faults that ruptured during the 1957 earthquake are the N–S striking Toromhon thrust faults that cut the lower Cretaceous sequence in the south of the Dulaan Bogd Pass area (Kurushin et al., 1998; Bayasgalan et al., 1999a; Point VII Fig. 3; Fig. 4j). These faults disappear northwards and absorb some of the displacement of the Bogd Fault system (Bayasgalan et al., 1999a).

A distinct, E–W striking thrust fault emplaces crystalline basement rocks over the Triassic–Jurassic volcano-sedimentary sequence (Point VIII and cross section A–A′ in Fig. 3; Fig. 4c, k). Some weak folding is observed in the Triassic–Jurassic sequence, which overall is dipping steeply southward. Interestingly, the thrust at the southern margin is steep, subparallel to the bedding of the Triassic–Jurassic rocks, and becomes low-angle towards the north. The low-angle part cuts down into the stratigraphy in the Triassic–Jurassic series (Fig. 4k), which requires that the Triassic–Jurassic beds were already tilted to the south at a higher angle than the thrust fault when thrusting started.

The thrust fault can be traced eastward, where it is bounded in the east by an N–S trending sidewall ramp (Point IX in Fig. 3). Absence of distinct markers does not allow conclusive assessment of the amount of displacement along the thrust fault, but the close comparison between the basement and the fan conglomerates in the Jurassic sequence that rework this sequence, as well as the rather short sidewall ramp suggests only small displacements, on the order of perhaps a hundred meters or less. The morphology of the thrust and the scree that overlies it in many places suggests that the fault was not activated during the 1957 earthquake. The N–S trending sidewall ramp further suggests that the thrust accommodated N–S shortening, and is not a transpressional feature such as the Bogd Fault described above.

To the west, the thrust fault can be traced throughout the map area, but in the valley ~10 km to the west of the Dulaan Bogd Pass area (Figs. 2 and 4m), the basement does not appear to overlie the Triassic–Jurassic stratigraphy. Instead, the geomorphology of the southern margin is strongly suggestive of a normal fault, displaying flat-irons and tilted fault block geometries (Fig. 4m), with bedding dipping steeply into the contact with the basement. In the north, the contact of the Triassic–Jurassic stratigraphy with the basement is subparallel with bedding, and is most likely depositional, similar to the contact observed at point I in Fig. 3.

Further evidence for shortening is found in two locations south and southeast of Jaran Bogd. Firstly, approximately 15 km to the southwest of the Dulaan Bogd pass, the lower Cretaceous stratigraphy is overlain by a thrust sheet consisting of white marbles belonging to the crystalline basement (Figs. 2 and 4n). Again, the thrust contact dips to the south at a lower angle than the underlying lower Cretaceous lavas, and the thrust thus cuts down-stratigraphy, requiring that the lower Cretaceous was already southwards prior to the onset of thrusting. The upper Cretaceous covers both the thrust sheet and unconformably overlies the tilted Cretaceous stratigraphy, and is not disrupted by this thrust: therefore thrusting occurred sometime in the middle Cretaceous.

Secondly, in the valley to the south of Jaran Bogd, a prominent, NW–SE trending monocline deforms the lower Cretaceous stratigraphy (Figs. 2 and 4h). Regionally, the bedding of the lower Cretaceous strikes ENE–WSW and dips 30–50° SSE. In the monocline, bedding strikes are NW–SE striking and dips are up to vertical, locally even overturning. Although monoclines can form above blind normal faults, the subvertical to even overturned bedding in this monocline suggests it is of contractional origin.

The monocline is covered by red clastic sediments which may correlate with the upper Cretaceous, and an undeformed lava plateau, the Jaran Plateau, which has a similar appearance and geochemistry as the ~30 Ma Bogd plateau to the east of Baga Bogd (Dupont-Nivet et al., 2010). We have tentatively mapped these volcanics as Paleogene, similar to Zabotkin (1988). The lavas of the Jaran Plateau post-date the formation of the monocline.

4. Geochronology

4.1. $^{40}Ar/^{39}Ar$ geochronology

4.1.1. Analytical protocol

Samples were crushed with a jaw crusher and sieved (mesh size 180–250 μm). A portion was set aside for whole-rock analysis. Conventional mineral separation techniques were employed to separate feldspars. The mineral separates were washed in acetone several times and finally in distilled water. Grains were handpicked under a binocular microscope. Mineral grains with grain coatings or inclusions were avoided. The samples were packed in aluminum capsules together with the Taylor Creek Rhyolite (TCR) flux monitor standard along with pure (zero age) K_2SO_4 and CaF_2 salts. The samples were irradiated together at IFE (Institutt for Energiteknikk, Kjeller, Norway) for 4.5 h with a nominal neutron flux of 1.3×10^{13} n·cm^{-2} ·s^{-1}. The correction factors for the production of isotopes from Ca were determined to be $(^{39}Ar/^{37}Ar)_{Ca} = (0.62523 \pm 0.04856) \times 10^{-3}$, $(^{36}Ar/^{37}Ar)_{Ca} = (0.59112 \pm 0.17343) \times 10^{-3}$ and $(^{40}Ar/^{39}Ar)_K = (1.7005302 \pm 0.3251701) \times 10^{-1}$ for the production of K (errors quoted at 1σ). The samples were step heated using a resistance furnace. The extracted gases were passed over hot (400 °C) SAES AP10 getters for the first 3 min, then for 9 min in a separate part of the extraction line with SAES AP-10 getters. They were analyzed with a MAP 215–50 mass spectrometer installed at the Geological Survey of Norway. The peaks were determined during peak hopping for 10 cycles (15 integrations pr. cycle) on the different masses ($^{41-5}$Ar) on a Balzers electron multiplier

and regressed back to zero inlet time. Blanks were analyzed before the analysis of the unknowns at different temperature steps and from those values we used interpolation to assign a blank for the different temperature levels. After blank correction, a correction for mass fractionation, ^{37}Ar and ^{39}Ar decay and neutron-induced interference reactions produced in the reactor was undertaken using in-house software (AgeMonster written by M. Ganerød). It implements the equations of McDougall and Harrison (1999) and the newly proposed decay constant for ^{40}K after Renne et al. (2010). A $^{40}Ar/^{36}Ar$ ratio of 298.56 ± 0.31 from Lee et al. (2006), was used for the atmospheric argon correction and mass fractionation calculation (power law). We calculated J-values relative to an age of 28.619 ± 0.034 Ma for the TCR sanidine flux monitor (Renne et al., 2010). Weighted mean ages are calculated by weighting on the inverse of the variance (analytical uncertainties).

4.1.2. Results

The results from the K-feldspars and the whole rock analysis from the analyzed samples of the Triassic–Jurassic (DB3) and Lower Cretaceous (JB7 and JB12) mafic lavas are shown in Table 1 and the spectra (with K/Ca ratios and $\%^{40}Ar^*$), and the inverse isochron results are displayed in Fig. 6. The raw isotopic dataset (corrected for blanks with propagated uncertainties) can be found in the supplemental dataset and follows the reporting norms of Renne et al. (2009). The results are quoted at the 1.96σ. Sample DB3 released gas in 19 steps where a weighted mean plateau age of 218.51 ± 1.48 Ma (MSWD = 1.019, P = 0.4) was calculated from 53.08% of the total ^{39}Ar. Excluding heating step 12 with negative ^{36}Ar (probably due to lowering of the blank level during measurement of the unknown) gives an inverse isochron age of 215.93 ± 3.42 Ma. Samples JB7 and JB12 released gas in 18 heating steps and defines stable plateaus in the middle of their spectra. A weighted mean plateau age of 124.15 ± 0.35 Ma (56.11%^{39}Ar, MSWD = 0.5, P = 0.8) and a weighted mean age of 123.19 ± 0.66 Ma (42.79%^{39}Ar, MSWD = 0.55, P = 0.7) for sample JB7 and JB12 respectively. The intercept of the inverse isochrons are difficult to calculate accurately and their uncertainties are large due to clustering of the data points (spread calculated after Jourdan et al. (2009)), so there could be loss or excess ^{40}Ar in the spectrum. However, the concordance between the spectrum ages and the inverse isochron ages seems to rule this out.

4.2. U/Pb geochronology

Zircons were extracted from sample DB1 obtained from the basement granitoid, using conventional mineral separation methods including the use of methylene iodide heavy liquid. Clean zircons were picked from the heavy mineral separate and mounted together with zircon standard CZ3 in a 2.5 cm diameter epoxy mount. The polished was imaged using a scanning electron microscope with a cathodoluminescence detector at Curtin University, Perth, Australia, and the sample was subsequently cleaned and gold-coated. Zircons resemble typical magmatic zircons with concentric and patchy zoning, without obvious xenocrystic cores. Zircons and zircon standards were analyzed for U, Pb and Th using a SHRIMP II ion microprobe at Curtin University. Before analysis, each site was cleaned by rastering the ion beam over the area of interest for 2 min. Data was processed using the Isoplot add-in for Excel (Ludwig, 1999). Zircons analyzed had overall high concentrations of U (511–1365 ppm). Three of the 7 zircons analyzed contained high concentrations of common Pb (4–12%), and two of these plot off the concordia at apparent 'young' $^{206}Pb/^{238}U$ ages between 440–375 Ma (Supplementary data). For the four remaining analyses with low common Pb, we used the measured ^{204}Pb to correct for common Pb, and these analyses lie on the concordia. Three of

Table 1
$^{40}Ar/^{39}Ar$ results for furnace step heating experiments. Ages are in Ma and uncertainties are reported as analytical errors at the 1.96σ level. Bold numbers are the preferred values, see text for explanation. MSWD (P) denotes mean squared weighted deviance and P is the probability of fit. TGA denotes Total Gas Age. The spread is calculated after the method in Jourdan et al. (2009). K/Ca is calculated from $^{39}Ar_k/^{37}Ar_{Ca}$.

Sample	Material	Lat	Long	Steps	Spectrum					Inverse isochron			
					$\%^{39}Ar$	Age ± 1.96σ	MSWD (P)	TGA ± 1.96σ	K/Ca ± 1.96σ	Age ± 1.96σ	MSWD (P)	Trapped $^{40}Ar/^{36}Ar$	Spread (%)
DB3	Feldspar	44°55.436′N	101°03.822′E	11–16 (6)	53.08	**218.51 ± 1.48**	1.02(0.4)	218.34 ± 1.51	1.03 ± 0.07	215.93 ± 3.42	0.745 (0.53)	−51.42 ± 61.38	0.3
JB7	Whole rock	44°52.792′N	100°43.712′E	9–15 (7)	56.11	124.15 ± 0.35	0.50(0.81)	124.02 ± 0.51	1.58 ± 0.17	**124.82 ± 1.15**	0.33 (0.9)	101.56 ± 139.94	0.3
JB12	Whole rock	44°50.746′N	100°44.617′E	6–10 (5)	42.79	**123.19 ± 0.66**	0.55(0.7)	118.88 ± 0.68	2.47 ± 0.22	122.66 ± 1.426	0.51(0.68)	342.83 ± 104.10	4

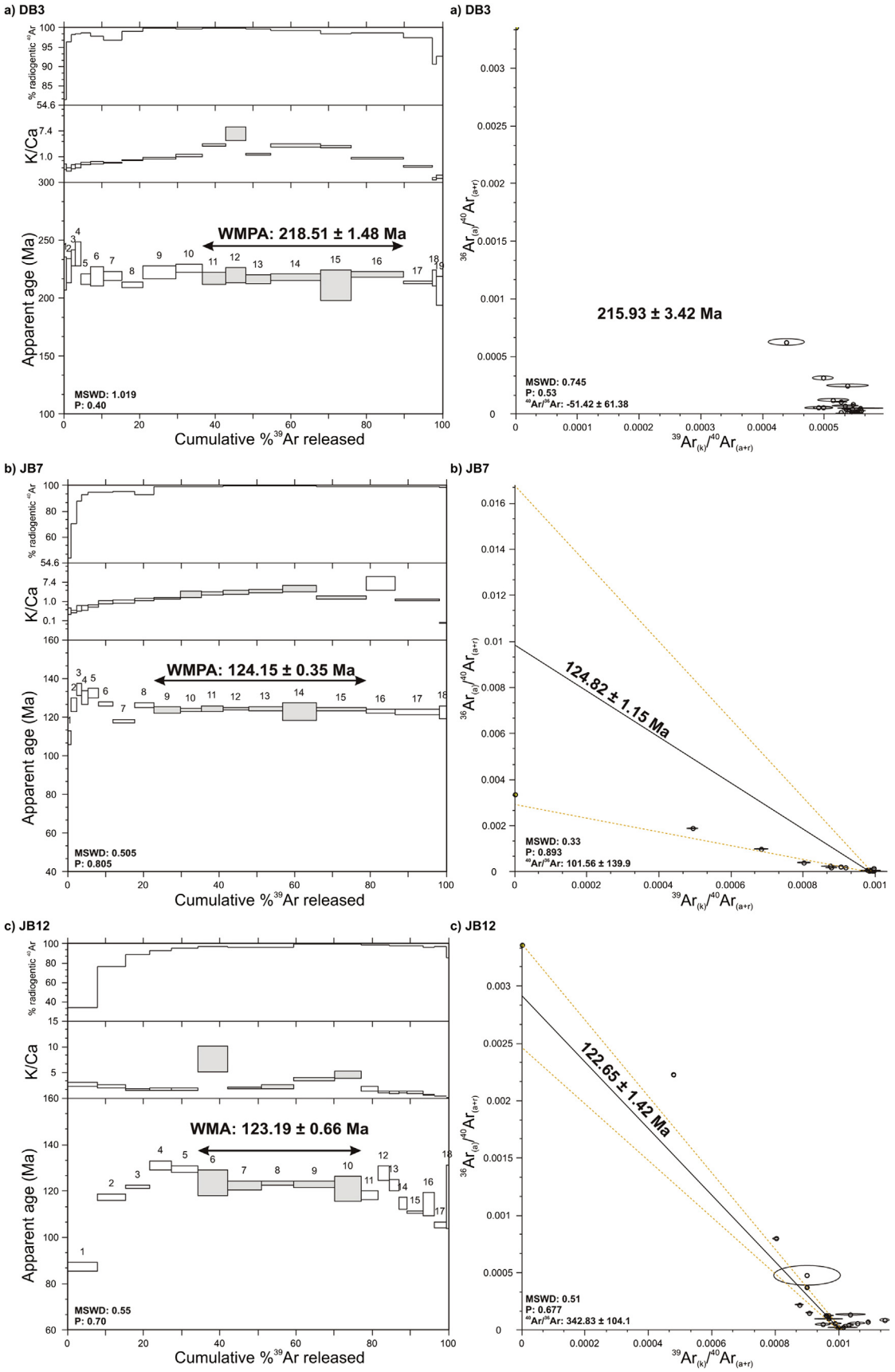

Figure 6. $^{40}Ar/^{39}Ar$ age spectrums (below) and K/Ca ratios (above) for furnace step heating experiments from sample (a) DB3, (b) JB7, and (c) JB12. The error bars at each step and the calculated ages are shown at the 95% confidence level (1.96σ). The numbers above each bar represent the experiment number in the supplemental data file.

these four define a ^{204}Pb-corrected ^{206}Pb/^{238}U concordia age of 502 ± 8 Ma (95% confidence level), with a probability of concordance of 0.72 and an MSWD of 0.97. The remaining analysis has a ^{204}Pb corrected ^{206}Pb/^{238}Pb age of 479 ± 6 Ma, perhaps recording continuous Pb loss during cooling of the intrusion. Because of the problems with common Pb in this sample, the age of 502 ± 8 should probably be considered as a minimum age for the intrusion. The data collected is reported in Table I in the supplementary files.

5. Discussion

5.1. Multi-phase deformation focused along the Bogd Fault area

Amalgamation of the continental crust of the study area by terrane accretion and magmatism occurred in Paleozoic times, as reviewed for the Baga Bogd region by Demoux et al. (2009). Our U/Pb age of zircons of the granites that are prominent in the Dulaan Bogd Pass area of 502 ± 8 Ma is very similar to the youngest granitoids reported by (Demoux et al., 2009) from the crystalline basement of Mt. Baga Bogd basement of ~502–498 Ma. Across Mongolia, the crystalline basement shows a very prominent curved structural trend from NW–SE in the west to NE–SW in the east (Badarch et al., 2002). In the study area, the dominant structures in the basement are E–W trending, sub-parallel to the Bogd Fault zone (Badarch et al., 2002).

Our results indicate that the study area experienced at least four phases of deformation in Mesozoic and Cenozoic time (Fig. 7). We have not observed growth faults and consequently, we need to infer the tectonic history of the study area from the few major structures reported above, in combination with the distribution and thickness of the sedimentary units. A first phase of deformation must have occurred during the deposition of the Triassic–Jurassic lavas and sediments. This phase started around ~220 Ma based on the ^{40}Ar/^{39}Ar ages reported in this paper, and a similar age reported from the Tugrug basin to the NE (Johnson et al., 2014), and may have continued to at least ~190 Ma, assuming that the lavas that overlie basement on the summit of Ih Bogd reported previously by Jolivet et al. (2007) form part of the same sequence.

In the Dulaan Bogd Pass area, these deposits are more than 1 km thick, and unconformably overlie basement in the north. Paleocurrent directions show that the main depocenter was in the south of the basin, and the coarse, angular conglomerates near the top of the stratigraphy in the south shows that despite 1 km of sediment infill, there was still basement available for erosion at short distance from the southern basin margin. Presently, the basin is bounded in the south by a thrust. We consider it unlikely, however, that this fault is responsible for the formation of the accommodation space that formed the basin. Firstly, the thrust cuts down-section and hence post-dates southward tilting of the stratigraphy. If the Triassic–Jurassic basin was a foreland basin filled during thrusting, the thrust can only cut up-section.

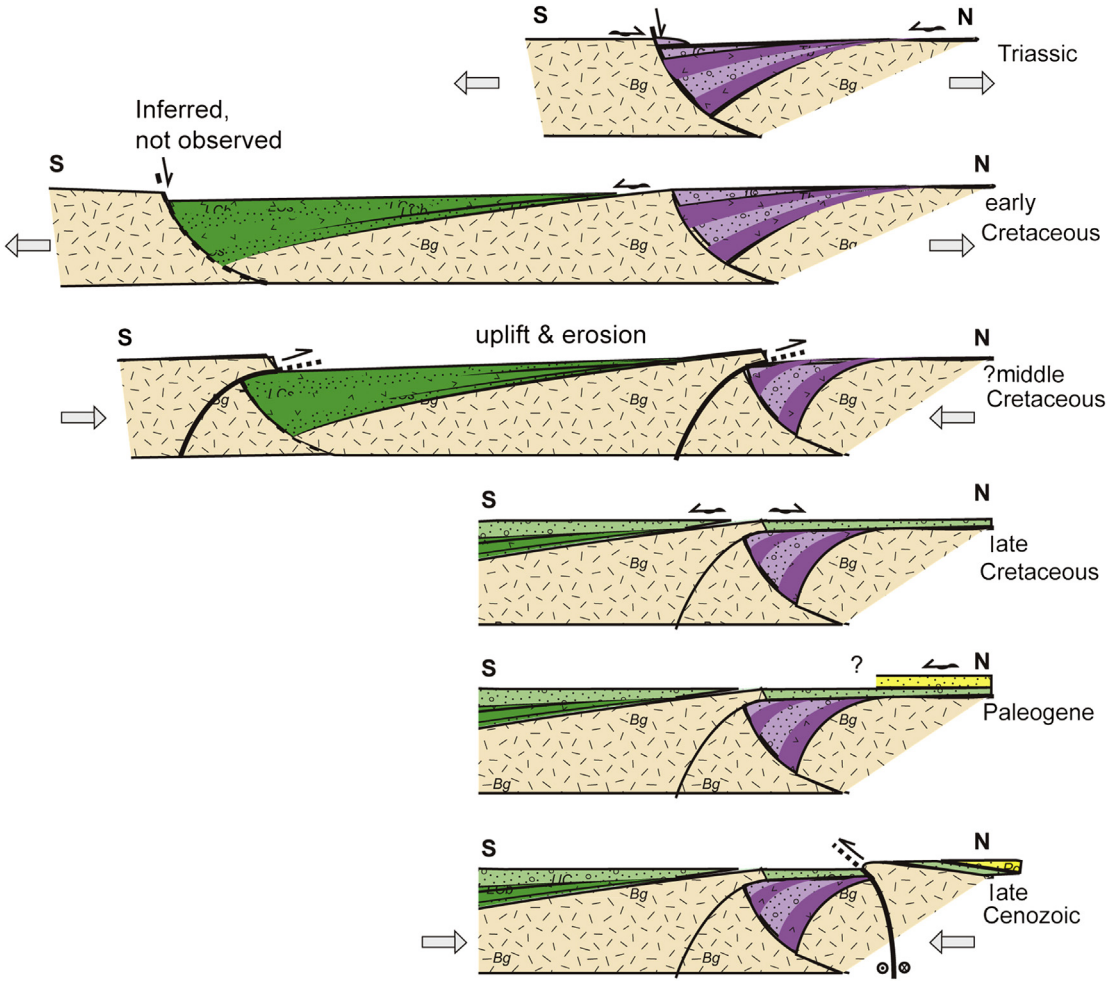

Figure 7. Interpreted tectonic evolution for the Dulaan Bogd Pass and Jaran Bogd areas. The composite section is approximately located along section A–A′ for the northern basin, and where the basement overthrusts over lower Cretaceous lavas, 10 km to the SW (see Figs. 2 and 4n for location).

We consider it more likely that the Triassic–Jurassic basin was an E–W trending half-graben bounded in the south by a high-angle, north-dipping normal fault (Fig. 7). The geomorphology of the valley ~10 km to the west suggests that normal faults along the southern margin of the Triassic–Jurassic basin are still preserved. Normal faulting created the southward back-tilting that hence existed when thrusting started.

We infer a history that is quite similar for the deposition of the lower Cretaceous lava and sediment series that were deposited between ~125 and ~115 Ma ago (based on the $^{40}Ar/^{39}Ar$ ages reported in this paper, and in van Hinsbergen et al., 2008), and those of Barry (1999) from lavas on the southern flanks of Artza Bogd further east (Fig. 1). The lower Cretaceous sequence is gently tilted to the SSE by ~15° in the Dulaan Bogd pass area, but dip gradually increases to ~40–50° in the Jaran Bogd area ~25 km to the west of the Dulaan Bogd Pass. The sequence thickens from ~100 m in the Dulaan Bogd Pass area to at least 1500 m in the Jaran Bogd section (Figs. 2 and 5). Moreover, the lower Cretaceous flow units thin and disappear eastwards in the Dulaan Bogd Pass region (Fig. 3). This suggests that the Dulaan Bogd Pass is close to the former eastern margin of an early Cretaceous extensional basin, which had a depocenter in the Jaran Bogd area.

Similar to the Triassic–Jurassic basin, the lower Cretaceous lavas are overthrust in the south by crystalline basement, and this thrust cuts down-section. Consequently, we infer that southward tilting of the stratigraphy pre-dated thrusting. Although we have no direct observational evidence to confirm extensional displacement, we suggest that the ~125–120 Ma creation of ~1500 m of accommodation space was related to ~N–S extension that formed a north-dipping normal fault to the south of the basin (Fig. 7). Exposures of crystalline basement directly to the south of the lower Cretaceous suggests that this fault likely existed near the current exposures of the lower Cretaceous, although later thrusting has obscured the exact location. Cunningham et al. (2009) documented contemporaneous N–S extension in the Nemegt Uul region, ~100 km to the south of the study area. The NW–SE extension documented in the Tugrug basin to the northeast created a sedimentary basin with similar stratigraphic thickness, but developed somewhat earlier, between ~155–140 Ma (Johnson et al., 2014).

A phase of ~N–S or NE–SW shortening must have affected the study area sometime after the deposition of the lower Cretaceous and prior to the deposition of the red conglomerates regionally assigned to the upper Cretaceous, as well as prior to the deposition of the Jaran Plateau lavas. Although direct age information in the study areas is lacking, we infer that thrusting and monocline formation in the Jaran Bogd area occurred sometime in the mid-Cretaceous. We tentatively ascribe the thrust that brought crystalline basement over the Triassic–Jurassic stratigraphy to the same deformation phase (Fig. 7), although direct cross-cutting relationships are absent for this structure. It is unclear why the rift basins were overthrusted from the south instead of simply shortened by reactivation of their bounding normal faults in thrust mode. The structural grain exposed in low-grade metamorphic basement directly south of the study area is regionally south dipping and this may have provided a favorably oriented mechanical anisotropy for deeper initiation of north-directed over-thrusting during Cretaceous shortening.

Following this phase of crustal shortening, the upper Cretaceous coarse clastic formation was deposited with an angular unconformity on all previous units. On a regional scale, these conglomerates are subhorizontal, only modified locally along zones of deformation associated with Cenozoic strike-slip/transpression. These deposits do not attain very large thicknesses in the study area (<100 m), and we do not infer a phase of deformation that led to their deposition. Rather, they appear to fill a paleorelief of basement and older Mesozoic sediments. In the Dulaan Bogd Pass, the upper Cretaceous conglomerates are locally derived and are shed to the north in the north, and to the south in the south suggesting that the Dulaan Bogd Pass area formed a local high following the mid Cretaceous phase of thrusting (Fig. 7). This phase of mid-Cretaceous shortening was also interpreted from the seismic section of the Tugrug basin (Johnson et al., 2014).

Based on the available data, we cannot constrain the cause of the onset and cessation of upper Cretaceous sedimentation. Following this phase of sedimentation in the Dulaan Bogd Pass, the region was peneplaned, followed by deposition of the Paleogene distal conglomerates of a northerly provenance. The southward paleocurrent directions, together with the absence in the Paleogene conglomerates of any pebbles resembling the crystalline basement or its pre-Paleogene sedimentary cover suggests that these regions were not elevated and available for erosion.

Finally, during the late Cenozoic, the Gobi Altai was subjected to sinistral strike-slip and thrust displacements which generated uplift of the Baga Bogd and Ih Bogd restraining bends (Bayasgalan et al., 1999a; Cunningham, 2005, 2010, 2013; Vassallo et al., 2005, 2007a). In the Dulaan Bogd Pass area, this phase of deformation is best reflected by the mapped faults that ruptured during the 1957 earthquake (Fig. 7). A few kilometers to the south of the mapped area, N-dipping Quaternary faults with thrust displacements were inferred based on topographic steps and visual scarps on high-resolution satellite imagery (Cunningham, 2013).

The similarity between the cover stratigraphy and basement units across the strike-slip fault that ruptured in 1957 suggests that the cumulative displacement along this fault at this location is likely minor and perhaps on the order of a km or less. If considerable displacement has been accommodated along the Bogd Fault system farther to the west, most of this displacement must have been absorbed by thrust and oblique-slip displacements that generated Ih Bogd and other ranges west of the Dulaan Bogd Pass area. Thrust accommodation associated with the Bogd Fault has been described in the study area (Toromhon thrusts, Figs. 3 and 4j), as well as to the east of the Baga Bogd and Artz Bogd restraining bends (Bayasgalan et al., 1999a).

In summary, we interpret the structure and stratigraphy of the study area to reflect the following geological stages: (1) 220–190 Ma: N–S extension creating a north-facing half graben along a normal fault close to the northern slopes of the modern Ih Bogd. The basin is at least ~15 km wide and is filled with ~1 km mafic lavas and continental clastics; (2) ~125–115 Ma: ~N–S extension creating a north-facing half-graben along a normal fault close to the southern slopes of the modern Ih Bogd. The basin is at least 25 km wide and is filled with 1.5 km of mafic lavas, continental clastics, and lacustrine clays; (3) ?middle Cretaceous: N–S to NE–SW shortening, emplacing crystalline basement rocks over the Triassic–Jurassic stratigraphy, as well as the lower Cretaceous stratigraphy; (4) upper Cretaceous–Paleogene: tectonic quiescence, erosion and peneplanation. Upper Cretaceous sediments fill relative low areas and are locally sourced, Paleogene conglomerates are far-traveled; (5) late Neogene (since 8 ± 3 Ma; Vassallo et al., 2007a): uplift of the Ih Bogd and Baga Bogd restraining bends along the Bogd left-lateral strike-slip system. Cumulative strike-slip displacements along this fault in the study area may be on the order of a kilometer or less, and the study area is near the eastern termination of this fault zone (Bayasgalan et al., 1999a).

5.2. Regional implications and plate kinematic context

Our analysis shows that throughout the Mesozoic and Cenozoic eras, extensional, compressional, and transcurrent deformation has

occurred in the northern Gobi Altai region, and the structures that formed during these stages are parallel to the main strike trends in the Paleozoic and older crystalline basement. Although the faults that formed in each episode have separate surface expressions, which appear not to be reactivated, we suspect that deeper seated weak zones in the underlying Paleozoic crust are reactivated in each stage and are responsible for the focusing of deformation.

Although all deformation stages are associated with minor fault displacements on the order of a few kilometers, and generally less, our results provide some age constraints for each episode. Our study area may then serve as a further constraint on the widely discussed long-lived intra-plate deformation history of Central Asia.

Regional, widely distributed deformation requires an explanation and several scenarios have been proposed to explain the very widely distributed Triassic–Cretaceous intra-plate magmatic and tectonic history of Mongolia. These include driving mechanisms such as regional gravitational collapse following crustal thickening and mountain building to the north (Mongol-Okhotsk suture) and south (Yinshan-Yanshan mountain belt in northern China; Graham and Hendrix, 2001; Johnson et al., 2001; Meng, 2003; Meng et al., 2003), back-arc extension in the hinterland of the Pacific active margin, (e.g. Watson et al., 1987; Davis et al., 1998) or continental scale lithospheric delamination following closure of the Mongol-Okhotsk ocean (Wang et al., 2006).

Fig. 8 shows the position of our field area relative to the plate boundaries as they probably existed at 220 Ma and 120 Ma according to a recent plate model for the closure of the Mongol-Okhotsk ocean of Van der Voo et al. (2015). Deformation in the late Triassic to early Jurassic is widespread in Mongolia, and comes in different styles: N–S compression to the south of our study area (Hendrix et al., 1996; Zheng et al., 1996; Lamb et al., 2008; Rippington et al., 2013; Guy et al., 2014), N–S extension to the southeast in northern China (Meng et al., 2014), and major transcurrent faulting along the East-Gobi sinistral shear zone to the east (Webb et al., 2010). The Gobi Altai area during that time was near enough to subduction plate boundaries to have been directly affected by plate margin processes. The western termination of the Mongol-Okhotsk suture and subduction zone is not well determined, but may have been within ~200 km north of the study area, with the Ih Bogd-Baga Bogd region located in an overriding plate position to the southern limb of a double-vergent subduction zone (see Zorin, 1999; Bussien et al., 2011, and references therein). In addition, the study area is located within 500 km north of the Solonker Suture, where convergence may have continued until the middle Triassic (Xiao et al., 2010; Rippington et al., 2013). Although we see insufficient grounds to propose a detailed kinematic and dynamic explanation for the Triassic–Jurassic extension that we infer from our study area, we suspect that this explanation is found in the context of nearby subduction and collision zone activity, or as a response to the termination of their activity. For a broader discussion on the early mid-Mesozoic sedimentary basins of Mongolia, we refer to Johnson (2015), who recently suggested that these basins may relate to regional strike-slip tectonics associated with relative rotations between Mongolia, China and Siberia during closure of the Mongol-Okhotsk ocean.

The Cretaceous extension phase is also challenging to explain. The extension that we infer, and the volcanism that we have dated falls in a regionally well-constrained and very extensive, long-lasting (~60 Myr) phase of extension that is reported throughout Mongolia and parts of China over an area of ~1000 km × 1000 km. This deformation is truly intra-plate: to the south, the distance of our study area to the Tethyan subduction zone around 120 Ma was 2500 km (taking Tibetan shortening into account as reconstructed in van Hinsbergen et al. (2011)); to the east, the distance to the Pacific subduction zone was ~2700 km; to the north, the nearest plate boundary at that time was in the Canada Basin, over 6000 km away; and to the west the nearest plate boundary was the central Atlantic Ocean, >7000 km away (Fig. 8). It is unlikely that this extension was related to the dynamics of a single plate boundary (e.g., Meng et al., 2003; Johnson and Ritts, 2012; Johnson, 2015). To illustrate the dimensions of the problem: the extensional deformation in Mongolia is at a distance from the nearest subduction zone that is similar to the distance of Denmark from the Mediterranean subduction zone, or the distance of Florida from the Pacific subduction zone in Mexico.

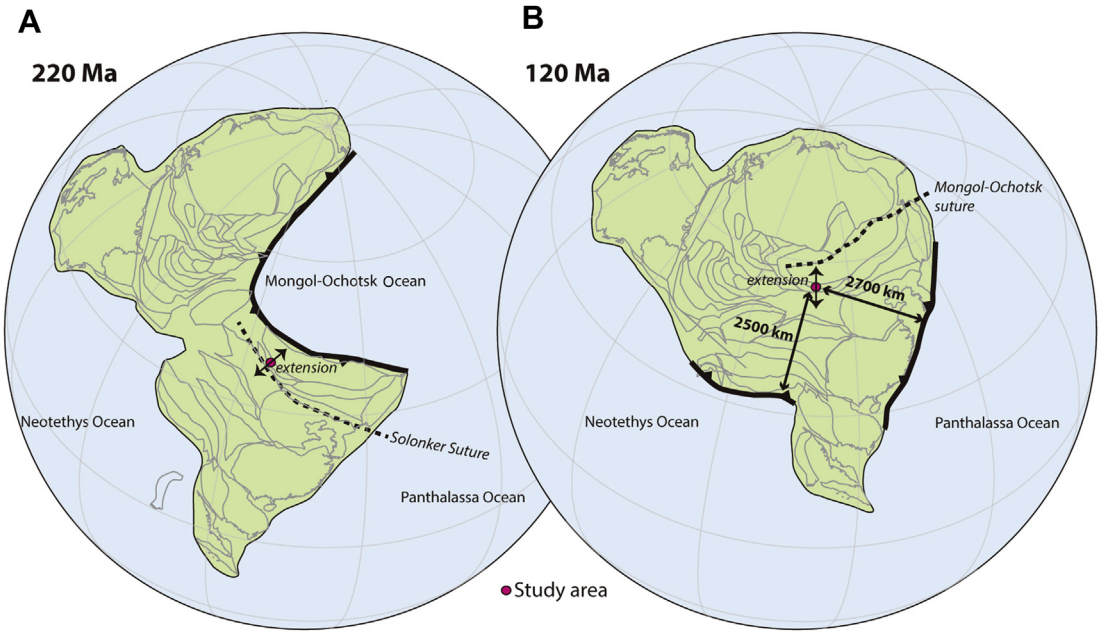

Figure 8. Location of the field area relative to the nearest plate boundaries at (A) 220 Ma and (B) 120 Ma. Reconstructions from Van der Voo et al. (2015).

We consider it more likely that the widely distributed deformation in Mongolia, is explained by interaction of all stresses transmitted from all plate boundaries, in combination with tractions at the base of the lithosphere as a result of plate motion relative to the mantle, and stresses associated with dynamic topography resulting from the Mongol-Okhotsk slab sinking into the mantle below Mongolia. A similar explanation was recently put forward for the intra-plate stress fields of Africa (e.g., Gaina et al., 2013) or Eurasia (e.g., Warners-Ruckstuhl et al., 2010). Our field study highlights that intraplate deformation in Mongolia was accommodated along structures parallel to the regional basement grain throughout the Mesozoic and Cenozoic. The explanation for why intraplate deformation is so widespread in Mongolia and northern China, but not in cratonic Siberia or North China, must lie in the mechanical weakness and heterogeneity of its non-cratonic Phanerozoic terrane mosaic basement that contains weak fault and fabric belts that are more easily reactivated by far-field stresses (c.f., Webb and Johnson, 2006; Webb et al., 2010; Johnson and Ritts, 2012; Cunningham, 2013).

6. Conclusions

The Gobi Altai region of southern Mongolia is well known for its young transpression-related mountain building, but the depositional setting of the widespread Mesozoic deposits is less well constrained. In this paper, we further document and date the tectonic history of the Gobi Altai by studying the stratigraphy and structure of Triassic to Cenozoic deposits flanking Mt Ih Bogd that was constructed during late Neogene transpression.

Detailed mapping of the Dulaan Bogd Pass area revealed that during the Mesozoic Era, two prominent phases of basin formation occurred on top of crystalline basement that hosts a granitoid from which we provide a 502 ± 8 Ma U/Pb zircon age. North basin phases were characterized by fluvio-lacustrine deposition interrupted by volcanic episodes during which regionally extensive basalts were emplaced. We provide new $^{40}Ar/^{39}Ar$ feldspar ages from basalts showing that the first phase of basin formation was underway by 218.5 ± 1.5 Ma, and the second occurred during early Cretaceous time, with ages of 124.2 ± 0.4 and 123.2 ± 0.7 Ma. Both basins contain stratigraphic infill over 1 km thick that underwent southward tilting during deposition consistent with deposition in north-facing half-grabens during overall ~N–S extension. These episodes of extensional basin formation were followed by a less well constrained, but likely mid-Cretaceous phase of ~N–S contraction, leading to northward overthrusting of crystalline Paleozoic and older basement over basin deposits.

Our results shed further light on the widespread, episodic extensional history of central Asia in late Triassic and early Cretaceous time, and provide further field evidence for mid-Cretaceous shortening and basin inversion in Mongolia. This deformation was of low magnitude with cumulative displacements on the order of kilometers or less, but may place timing constraints on changes in the force balance along Eurasia's plate boundaries since the late Triassic.

Acknowledgments

This work was supported by UK NERC Grant NER/D/S/2003/00671 to WDC. The 2005 fieldwork of DJJvH was partly supported by an E.J. Garwood Grant of the Geological Society of London. GBS was supported by the Molengraaff Foundation and the KF Hein Foundation. DJJvH acknowledges funding through ERC Starting Grant 306810 (SINK) and an NWO VIDI grant. We thank Laura Webb and Cari Johnson for constructive reviews.

Appendix A. Supplementary data

Supplementary data related to this article can be found at http://dx.doi.org/10.1016/j.gsf.2014.12.002.

References

Allen, M.B., Vincent, S.J., 1997. Fault reactivation in the Junggar region, northwest China: the role of basement structures during Mesozoic-Cenozoic compression. Journal of the Geological Society 154, 151–155.
Badarch, G., Cunningham, W.D., Windley, B.F., 2002. A new terrane subdivision for Mongolia: implications for the Phanerozoic crustal growth of Central Asia. Journal of Asian Earth Sciences 21, 87–110.
Baljinnyam, I., Bayasgalan, A., Borisov, B.A., Cisternas, A., 1993. Ruptures of major earthquakes and active deformation in Mongolia and its surroundings. In: Geological Society of America Memoirs 181, p. 61.
Barry, T.L., 1999. Origins of Cenozoic Basalts in Mongolia; a Chemical and Isotope Study. Department of Geology. University of Leicester, Leicester.
Barry, T.L., Saunders, A.D., Kempton, P.D., Windley, B.F., Pringle, M.S., Dorjnamjaa, D., Saandar, S., 2003. Petrogenesis of cenozoic basalts from Mongolia: evidence for the role of Asthenospheric versus Metasomatized lithospheric mantle sources. Journal of Petrology 44, 55–91.
Bayarsayhan, C., Bayasgalan, A., Enhtuvshin, B., Hudnut, K.W., Kurushin, R.A., Molnar, P., Ölziybat, M., 1996. 1957 Gobi-Altay, Mongolia, earthquake as a prototype for southern California's most devastating earthquake. Geology 24, 579–582.
Bayasgalan, A., Jackson, J., Ritz, J.-F., Carretier, S., 1999a. Field examples of strike-slip fault terminations in Mongolia and their tectonic significance. Tectonics 18, 394–411.
Bayasgalan, A., Jackson, J., Ritz, J.F., Carretier, S., 1999b. Forebergs', flower structures, and the development of large intra-continental strike-slip faults: the Gurvan Bogd fault system in Mongolia. Journal of Structural Geology 21, 1285–1302.
Bussien, D., Gombojav, N., Winkler, W., Quadt von, A., 2011. The Mongol–Okhotsk Belt in Mongolia — An appraisal of the geodynamic development by the study of sandstone provenance and detrital zircons. Tectonophysics 510 (1–2), 132–150.
Choi, J.-H., Jin, K., Enkhbayar, D., Davvasambuu, B., Bayasgalan, A., Kim, Y.-S., 2012. Rupture propagation inferred from damage patterns, slip distribution, and segmentation of the 1957 M W8.1 Gobi-Altay earthquake rupture along the Bogd fault, Mongolia. Journal of Geophysical Research 117, B12401. http://dx.doi.org/10.1029/2011JB008676.
Cogne, J.-P., Kravchinsky, V.A., Halim, N., Hankard, F., 2005. Late Jurassic-Early Cretaceous closure of the Mongol-Okhotsk Ocean demonstrated by new Mesozoic palaeomagnetic results from the Trans-Baïkal area (SE Siberia). Geophysical Journal International 163, 813–832.
Cox, A., Hart, R.B., 1986. Plate Tectonics: How it Works. Blackwell Science.
Cunningham, D., 2010. Tectonic Setting and Structural Evolution of the Late Cenozoic Gobi Altai Orogen. Geological Society, London, pp. 361–387. Special Publications 338.
Cunningham, D., 2013. Mountain building processes in intracontinental oblique deformation belts: lessons from the Gobi Corridor, Central Asia. Journal of Structural Geology 46, 255–282.
Cunningham, W.D., 1998. Lithospheric controls on late Cenozoic construction of the Mongolian Altai. Tectonics 17, 891–902.
Cunningham, W.D., 2005. Active intracontinental transpressional mountain building in the Mongolian Altai: defining a new class of orogen. Earth and Planetary Science Letters 240, 436–444.
Cunningham, W.D., Davies, S.J., McLean, D., 2009. Exhumation of a Cretaceous rift complex within a Late Cenozoic restraining bend, southern Mongolia: implications for the crustal evolution of the Gobi Altai region. Journal of the Geological Society 166, 321–333.
Cunningham, W.D., Windley, B.F., Owen, L.A., Barry, T., Dornjnamjaa, D., Badamgarav, J., 1997. Geometry and style of partitioned deformation within a late Cenozoic transpressional zone in the eastern Gobi Altai Mountains, Mongolia. Tectonophysics 277, 285–306.
Daoudene, Y., Gapais, D., Ledru, P., Cocherie, A., Hocquet, S., Donskaya, T.V., 2009. The Ereendavaa range (north-eastern Mongolia): an additional argument for Mesozoic extension throughout eastern Asia. International Journal of Earth Sciences 98, 1381–1393.
Daoudene, Y., Gapais, D., Ruffet, G., Gloaguen, E., 2012. Syn-thinning pluton emplacement during Mesozoic extension in eastern Mongolia. Tectonics 31. http://dx.doi.org/10.1029/2011TC002926 p. TC3001.
Davis, G.A., Cong, W., Yadong, Z., Jinjiang, Z., Changhou, Z., Gehrels, G.E., 1998. The enigmatic Yinshan fold-and-thrust belt of northern China: new views on its intraplate contractional styles. Geology 26, 43–46.
Demoux, A., Kröner, A., Liu, D., Badarch, G., 2009. Precambrian crystalline basement in southern Mongolia as revealed by SHRIMP zircon dating. International Journal of Earth Sciences 98 (6), 1365–1380.
Dewey, J.F., Shackleton, R.M., Chengfa, C., Yiyin, S., 1988. The tectonic evolution of the Tibetan Plateau. Philosophical Transactions of the Royal Society A 327, 379–413.
Dickinson, W., Snyder, W., 1978. Plate tectonics of the Laramide orogeny. In: Geological Society of America Memoirs 151, pp. 355–366.

Donskaya, T.V., Gladkochub, D.P., Mazukabzov, A.M., Ivanov, A.V., 2013. Late Paleozoic – Mesozoic subduction-related magmatism at the southern margin of the Siberian continent and the 150 million-year history of the Mongol-Okhotsk Ocean. Journal of Asian Earth Sciences 62, 79–97.

Dupont-Nivet, G., van Hinsbergen, D.J.J., Torsvik, T.H., 2010. Persistently low Asian paleolatitudes: implications for the India-Asia collision history. Tectonics 29. http://dx.doi.org/10.1029/2008TC002437. TC5016.

Faccenna, C., Becker, T.W., Auer, L., Billi, A., Boschi, L., Brun, J.-P., Capitanio, F.A., Funiciello, F., Horvàth, F., Jolivet, L., Piromallo, C., Royden, L., Rossetti, F., Serpelloni, E., 2014. Mantle dynamics in the Mediterranean. Reviews of Geophysics. http://dx.doi.org/10.1002/2013RG000444.

Fanti, F., Currie, P.J., Badamgarav, D., 2012. New Specimens of Nemegtomaia from the Baruungoyot and Nemegt formations (Late Cretaceous) of Mongolia. PLoS ONE 7, e31330.

Florensov, N.A., Solonenko, V.P., 1963. The Gobi-altai Earthquake. Akademiya Nauk USSR, Moscow (in Russian; English translation, 1965): U.S. Department of Commerce, Washington DC.

Gaina, C., Torsvik, T.H., van Hinsbergen, D.J.J., Medvedev, S., Werner, S.C., Labails, C., 2013. The African Plate: a history of oceanic crust accretion and subduction since the Jurassic. Tectonophysics 604, 4–25. http://dx.doi.org/10.1016/j.tecto.2013.05.037.

Graham, S.A., Hendrix, M.S., 2001. Sedimentary record and tectonic implications of Mesozoic rifting in southeast Mongolia. In: Geological Society of America Bulletin.

Graham, S.A., Cope, T., Johnson, C.L., Ritts, B.D., 2012. Sedimentary Basins of the Late Mesozoic Extensional Domain of China and Mongolia. In: Phanerozoic Rift Systems and Sedimentary Basins. Elsevier B.V., pp. 443–461.

Guy, A., Schulmann, K., Clauer, N., Hasalová, P., Seltmann, R., Armstrong, R., Lexa, O., Benedicto, A., 2014. Late Paleozoic–Mesozoic tectonic evolution of the Trans-Altai and South Gobi Zones in southern Mongolia based on structural and geochronological data. Gondwana Research 25, 309–337.

Hendrix, M.S., Graham, S.A., Amory, J.Y., 1996. Noyon Uul syncline, southern Mongolia: lower Mesozoic sedimentary record of the tectonic amalgamation of central Asia. In: Geological Society of America Bulletin 108, pp. 1256–1274.

Heumann, M.J., Johnson, C.L., Webb, L.E., Taylor, J.P., 2014. Total and incremental left-lateral displacement across the East Gobi Fault Zone, southern Mongolia: Implications for timing and modes of polyphase intracontinental deformation. Earth and Planetary Science Letters 392, 1–15.

Howard, J.P., Cunningham, W.D., Davies, S.J., 2006. Competing processes of clastic deposition and compartmentalized inversion in an actively evolving transpressional basin, western Mongolia. Journal of the Geological Society of London 163, 657–670.

Howard, J.P., Cunningham, W.D., Davies, S.J., Dijkstra, A.H., Badarch, G., 2003. The stratigraphic and structural evolution of the Dzereg Basin, western Mongolia: clastic sedimentation, transpressional faulting and basin destruction in an intraplate, intracontinental setting. Basin Research 15, 45–72.

Höck, V., Daxner-Höck, G., Schmid, H.P., Badamgarav, D., Frank, W., Furtmüller, G., Montag, O., Barsbold, R., Khand, Y., Sodov, J., 1999. Oligocene-Miocene sediments, fossils and basalts from the Valley of Lakes (Central Mongolia) – an integrated study. Mitteilungen der Österreicher Geolischer Gesellschaft 90, 83–125.

Jerzykiewicz, T., Russell, D.A., 1991. Late Mesozoic stratigraphy and vertebrates of the Gobi basin. Cretaceous Research 12, 345–377.

Johnson, C.L., 2004. Polyphase evolution of the East Gobi basin: sedimentary and structural records of Mesozoic-Cenozoic intraplate deformation in Mongolia. Basin Research 16, 79–99.

Johnson, C.L., 2015. Sedimentary basins in transition: distribution and tectonic settings of Mesozoic strata in Mongolia. In: Anderson, T.H., Didenko, A.N., Johnson, C.L., Khanchuk, A., MacDonald, J., Schwartz, J. (Eds.), Late Jurassic Margin of Laurasia – a Record of Faulting Accommodating Plate Rotation, Geological Society of America Special Paper (in press).

Johnson, C.L., Constenius, K.C., Graham, S.A., Mackey, G., Menotti, T., Payton, A., Tully, J., 2014. Subsurface evidence for late Mesozoic extension in western Mongolia: tectonic and petroleum systems implications. Basin Research. http://dx.doi.org/10.1111/bre.12073.

Johnson, C.L., Ritts, B.D., 2012. Chapter 28. Plate interior poly-phase basins. In: Busby, C., Azor Perez, A. (Eds.), Tectonics of Sedimentary Basins Recent Advances. Blackwell Publishing Ltd., pp. 567–583.

Johnson, C.L., Webb, L.E., Graham, S.A., Hendrix, M.S., Badarch, G., 2001. Sedimentary and structural records of late Mesozoic high-strain extension and strain partitioning, East Gobi basin, southern Mongolia. In: Geological Society of America Memoirs, v. 194, pp. 413–434.

Jolivet, L., Faccenna, C., 2000. Mediterranean extension and the Africa-Eurasia collision. Tectonics 19, 1095–1106.

Jolivet, M., Dominguez, S., Charreau, J., Chen, Y., Li, Y., Wang, Q., 2010. Mesozoic and Cenozoic tectonic history of the central Chinese Tian Shan: reactivated tectonic structures and active deformation. Tectonics 29. http://dx.doi.org/10.1029/2010TC002712.

Jolivet, M., Ritz, J.F., Vassallo, R., Larroque, C., Braucher, R., Todbileg, M., Chauvet, A., Sue, C., Arnaud, N., De Vicente, R., Arzhanikova, A., Arzhanikov, S., 2007. Mongolian summits: an uplifted, flat, but still preserved erosion surface. Geology 35, 871–874.

Jourdan, F., Marzoli, A., Bertrand, H., Cirilli, S., Tanner, L.H., Kontak, D.J., McHone, G., Renne, P.R., Bellieni, G., 2009. 40Ar/39Ar ages of CAMP in North America: implications for the Triassic–Jurassic boundary and the 40K decay constant bias. Lithos 110, 167–180.

Kapp, P., Yin, A., Harrison, T.M., Ding, L., 2005. Cretaceous-tertiary shortening, basin development, and volcanism in central Tibet. In: Geological Society of America Bulletin 117, pp. 865–878.

Kurushin, R.A., Bayasgalan, A., Ölziybat, M., Enhtuvshin, B., Molnar, P., Bayarsayhan, C., Hudnut, K.W., Lin, J., 1998. The surface rupture of the 1957 Gobi-Altay, Mongolia, earthquake. In: Geological Society of America Special Paper 320, pp. 1–144.

Lamb, M.A., Badarch, G., Navratil, T., Poier, R., 2008. Structural and geochronologic data from the Shin Jinst area, eastern Gobi Altai, Mongolia: Implications for Phanerozoic intracontinental deformation in Asia. Tectonophysics 451, 312–330.

Lee, J.Y., Marti, K., Severinghaus, J.P., Kawamura, K., Yoo, H.S., Lee, J.B., Kim, J.S., 2006. A redetermination of the isotopic abundances of atmospheric Ar. Geochimica et Cosmochimica Acta 70, 4507–4512.

Lehmann, J., Schulmann, K., Lexa, O., Corsini, M., Kröner, A., Stípská, P., Tomurhuu, D., Otgonbator, D., 2010. Structural constraints on the evolution of the Central Asian Orogenic Belt in SW Mongolia. American Journal of Science 310, 575–628.

Li, S., Wilde, S.A., He, Z., Jiang, X., Liu, R., Zhao, L., 2014. Triassic sedimentation and post-accretionary crustal evolution along the Solonker suture zone in Inner Mongolia, China. Tectonics 34. http://dx.doi.org/10.1002/2013TC003444.

Loope, D.B., Dingus, L., Swisher III, C.C., Minjin, C., 1998. Life and death in a Late Cretaceous dune field, Nemegt basin, Mongolia. Geology 26, 27–30.

Ludwig, K.R., 1999. Using Isoplot/Ex, Version 2, a Geochronological Toolkit for Microsoft Excel, Berkley Geochronology Center Special Publ: No. 1a.

Maridet, O., Daxner-Höck, G., Badamgarav, D., Göhlich, U.B., 2014. The eomyid rodents (Mammalia) from the Oligocene and Miocene of the Valley of Lakes (Central Mongolia). Paläontol Z. http://dx.doi.org/10.1007/s12542-014-0224-6.

McDougall, I., Harrison, T.M., 1999. Geochronology and Thermochronology by the 40Ar/39Ar Method. Oxford University Press, New York.

McKenzie, D.P., Parker, R.L., 1967. The North Pacific: an example of tectonics on a sphere. Nature 216, 1276–1280.

McQuarrie, N., Wernicke, B., 2005. An animated tectonic reconstruction of southwestern North America since 36 Ma. Geosphere 1 (3), 147–172,. http://dx.doi.org/10.1130/GES00016.S1.

Meng, Q.-R., 2003. What drove late Mesozoic extension of the northern China-Mongolia tract? Tectonophysics 369, 155–174.

Meng, Q.-R., Wei, H.-H., Wu, G.-L., Duan, L., 2014. Early Mesozoic tectonic settings of the northern North China craton. Tectonophysics 611, 155–166.

Meng, Q.R., Hu, J.M., Jin, J.Q., Zhang, Y., Xu, D.F., 2003. Tectonics of the late Mesozoic wide extensional basin system in the China–Mongolia border region. Basin Research 15, 397–415.

Molnar, P., Lyon-Caen, H., 1988. Some simple physical aspects of the support, structure, and evolution of mountain belts. In: Geological Society of America Special Paper 218, pp. 179–207.

Molnar, P., Tapponnier, P., 1975. Cenozoic tectonics of Asia: effects of a continental collision. Science 189, 419–426.

Oncken, O., Hindle, D., Kley, J., Elger, K., Victor, P., Schemmann, K., 2006. Deformation of the Central Andean upper plate system — facts, fiction, and constraints for plateau models. In: The Andes, Frontiers in Earth Sciences. Springer, Berlin Heidelberg, pp. 3–27.

Philip, H., Ritz, J.-F., 1999. Gigantic paleolandslide associated with active faulting along the Bogd fault (Gobi-Altay, Mongolia). Geology 27, 211–214.

Renne, P.R., Deino, A.L., Hames, W.E., Heizler, M.T., 2009. Data reporting norms for 40Ar/39Ar geochronology. Quaternary Geochronology 4, 346–352.

Renne, P.R., Mundil, R., Balco, G., Min, K., Ludwig, K.R., 2010. Joint determination of 40K decay constants and 40Ar*/40K for the Fish Canyon sanidine standard, and improved accuracy for 40Ar/39Ar geochronology. Geochimica et Cosmochimica Acta 74, 5349–5367.

Rippington, S., Cunningham, D., England, R., Hendriks, B., 2013. The crustal assembly of southern Mongolia: new structural, lithological and geochronological data from the Nemegt and Altan ranges. Gondwana Research 23, 1535–1553.

Ritts, B.D., Berry, A.K., Johnson, C.L., Darby, B.J., Davis, G.A., 2010. Early Cretaceous supra-detachment basins in the Hohhot metamorphic core complex, Inner Mongolia, China. Basin Research 22, 45–60.

Rizza, M., Ritz, J.F., Braucher, R., Vassallo, R., Prentice, C., Mahan, S.A., McGill, S., Chauvet, A., Marco, S., Todbileg, M., Demberel, S., Bourlès, D., 2011. Slip rate and slip magnitudes of past earthquakes along the Bogd left-lateral strike-slip fault (Mongolia). Geophysical Journal International 186, 897–927.

Saleeby, J., 2003. Segmentation of the Laramide Slab—evidence from the southern Sierra Nevada region. In: Geological Society of America Bulletin 115, pp. 655–668.

Schellart, W.P., Freeman, J., Stegman, D.R., Moresi, L., May, D., 2007. Evolution and diversity of subduction zones controlled by slab width. Nature 446, 308–311.

Sengör, A.M.C., Natal'in, B.A., Burtman, V.S., 1993. Evolution of the Altaid tectonic collage and Palaeozoic crustal growth in Eurasia. Nature 364, 299–306.

Sobel, E.R., Chen, J., Heermance, R.V., 2006. Late Oligocene–Early Miocene initiation of shortening in the Southwestern Chinese Tian Shan: implications for Neogene shortening rate variations. Earth and Planetary Science Letters 247, 70–81.

Sokoutis, D., Willingshofer, E., 2011. Decoupling during continental collision and intra-plate deformation. Earth and Planetary Science Letters 305, 435–444.

Traynor, J.J., Sladen, C., 1995. Tectonic and stratigraphic evolution of the Mongolian People's Republic and its influence on hydrocarbon geology and potential. Marine and Petroleum Geology 12, 35–52.

van der Meer, D.G., Spakman, W., van Hinsbergen, D.J.J., Amaru, M.L., Torsvik, T.H., 2010. Towards absolute plate motions constrained by lower-mantle slab remnants. Nature Geoscience 3, 36–40.

Van der Voo, R., Spakman, W., Bijwaard, H., 1999. Mesozoic subducted slabs under Siberia. Nature 397, 246–249.

Van der Voo, R., van Hinsbergen, D.J.J., Domeier, M., Spakman, W., Torsvik, T.H., 2015. Latest Jurassic-earliest Cretaceous closure of the Mongol-Okhotsk Ocean: a paleomagnetic and seismological-tomographic analysis. In: Anderson, T.H., Didenko, A.N., Johnson, C.L., Khanchuk, A., MacDonald, J., Schwartz, J. (Eds.), Geological Society of America Special Paper (in press).

van Hinsbergen, D.J.J., Kapp, P., Dupont-Nivet, G., Lippert, P.C., DeCelles, P.G., Torsvik, T.H., 2011. Restoration of Cenozoic deformation in Asia, and the size of Greater India. Tectonics 30, TC5003. http://dx.doi.org/10.1029/2011TC002908.

van Hinsbergen, D.J.J., Straathof, G.B., Kuiper, K.F., Cunningham, W.D., Wijbrans, J., 2008. No vertical axis rotations during Neogene transpressional orogeny in the NE Gobi Altai: coinciding Mongolian and Eurasian early Cretaceous apparent polar wander paths. Geophysical Journal International 173, 105–126.

van Hinsbergen, D.J.J., Vissers, R.L.M., Spakman, W., 2014. Origin and consequences of western Mediterranean subduction, rollback, and slab segmentation. Tectonics 33, 393–419. http://dx.doi.org/10.1002/tect.20125.

Van Itterbeeck, J., Horne, D.J., Bultynck, P., 2005. Stratigraphy and palaeoenvironment of the dinosaur-bearing Upper Cretaceous Iren Dabasu formation, Inner Mongolia, People's Republic of China. Cretaceous Research 26, 699–725.

Vassallo, R., Jolivet, M., Ritz, J.F., Braucher, R., Larroque, C., Sue, C., Todbileg, M., Javkhlanbold, D., 2007a. Uplift age and rates of the Gurvan Bogd System (Gobi-Altay) by apatite fission track analysis. Earth and Planetary Science Letters 259, 333–346.

Vassallo, R., Ritz, J.-F., Braucher, R., Carretier, S., 2005. Dating faulted alluvial fans with cosmogenic10Be in the Gurvan Bogd mountain range (Gobi-Altay, Mongolia): climatic and tectonic implications. Terra Nova 17, 278–285.

Vassallo, R., Ritz, J.F., Braucher, R., Jolivet, M., Carretier, S., Larroque, C., Chauvet, A., Sue, C., Todbileg, M., Bourlès, D., Arzhannikova, A., Arzhannikov, S., 2007b. Transpressional tectonics and stream terraces of the Gobi-Altay, Mongolia. Tectonics 26, TC5013. http://dx.doi.org/10.1029/2006TC002081.

Vincent, S.J., Allen, M.B., 2001. Sedimentary record of Mesozoic intracontinental deformation in the eastern Junggar Basin, northwest China: response to orogeny at the Asian margin. In: Geological Society of America Memoir 194, pp. 341–360.

Vislobokova, I., Daxner-Höck, G., 2002. Oligocene-Early Miocene Ruminants from the Valley of Lakes (Central Mongolia). Annalen des Naturhistorischen Museums in Wien 103, 213–235.

Wang, F., Zhou, X.-H., Zhang, L.-C., Ying, J.-F., Zhang, Y.-T., Fu-Yuan, W., Zhu, R.X., 2006. Late Mesozoic volcanism in the Great Xing'an Range (NE China): timing and implications for the dynamic setting of NE Asia. Earth and Planetary Science Letters 251, 179–198.

Warners-Ruckstuhl, K.N., Meijer, P.T., Govers, R., Wortel, M.J.R., 2010. A lithosphere-dynamics constraint on mantle flow: analysis of the Eurasian plate. Geophysical Research Letters 37, L18308. http://dx.doi.org/10.1029/2010GL044431.

Watson, M.P., Hayward, A.B., Parkinson, D.N., Zhang, Z.M., 1987. Plate tectonic history, basin development and petroleum source rock deposition onshore China. Marine and Petroleum Geology 4, 205–225.

Webb, L.E., Johnson, C.L., 2006. Tertiary strike-slip faulting in southeastern Mongolia and implications for Asian tectonics. Earth and Planetary Science Letters 241, 323–335.

Webb, L.E., Johnson, C.L., Minjin, C., 2010. Late Triassic sinistral shear in the east gobi fault zone, Mongolia. Tectonophysics 495, 246–255.

Wilhem, C., Windley, B.F., Stampfli, G.M., 2012. The Altaids of Central Asia: a tectonic and evolutionary innovative review. Earth Science Reviews 113, 303–341.

Xiao, W.J., Huang, B., Han, C., Sun, S., Li, J., 2010. A review of the western part of the Altaids: a key to understanding the architecture of accretionary orogens. Gondwana Research 18, 253–273.

Xiao, W.J., Zhang, L.-C., Qin, K.-Z., Sun, S., Li, J.-L., 2004. Paleozoic accretionary and collisional tectonics of the eastern Tianshan (China): Implications for the continental growth of central Asia. American Journal of Science 304, 370–395.

Yin, A., Harrison, T.M., 2000. Geologic evolution of the Himalayan-Tibetan orogen. Annual Review of Earth and Planetary Sciences 28, 211–280.

Yin, A., Nie, S., Craig, P., Harrison, T.M., Ryerson, F.J., 1998. Late Cenozoic tectonic evolution of the southern Chinese Tian Shan. Tectonics 17, 1–27.

Zabotkin, L.B., 1988. Geological Map L47-XXX, 1:200,000. Open File Report, Geological Funds of Mongolia, Ulaanbaatar, Mongolia in Russian.

Zheng, Y., Zhang, Q., Wang, Y., Liu, R., Wang, S.G., 1996. Great Jurassic thrust sheets in Beishan (North Mountains)—Gobi areas of China and southern Mongolia. Journal of Structural Geology 18, 1111–1126.

Zhou, Y., Ji, Y., Pigott, J.D., Meng, Q., Wan, L., 2014. Tectono-stratigraphy of Lower Cretaceous Tanan sub-basin, Tamtsag Basin, Mongolia: sequence architecture, depositional systems and controls on sediment infill. Marine and Petroleum Geology 49, 176–202.

Zhou, Y.-Z., Han, B.-F., Zhang, B., Xu, Z., Ren, R., Li, X.-W., Su, L., 2012. The Yingba shear zone on the Sino-Mongolian border: southwestern extension of the Zuunbayan Fault from Mongolia to China and implications for Late Mesozoic intracontinental extension in Eastern Asia. Tectonophysics 574–575, 118–132.

Ziegler, P.A., Cloetingh, S., van Wees, J.-D., 1995. Dynamics of intra-plate compressional deformation: the Alpine foreland and other examples. Tectonophysics 252, 7–59.

Zorin, Y.A., 1999. Geodynamics of the western part of the Mongolia-Okhotsk collisional belt, Trans-Baikal region (Russia) and Mongolia. Tectonophysics 306 (1), 33–56.